NANOTRIBOLOGICAL PROPERTIES OF GRAPHENE GROWN BY CHEMICAL VAPOR DEPOSITION AND TRANSFERRED ONTO SILICON OXIDE SUBSTRATES

A THESIS SUBMITTED TO

THE GRADUATE SCHOOL OF ENGINEERING AND SCIENCE

OF BILKENT UNIVERSITY

IN PARTIAL FULFILLMENT OF THE REQUIREMENTS FOR

THE DEGREE OF

MASTER OF SCIENCE

IN

MECHANICAL ENGINEERING

By

Tuna Demirbaş

October, 2015

NANOTRIBOLOGICAL PROPERTIES OF GRAPHENE GROWN BY CHEMICAL VAPOR DEPOSITION AND TRANSFERRED ONTO SILICON OXIDE SUBSTRATES

By Tuna Demirbaş

October, 2015

We certify that we have read this thesis and that in our opinion it is fully adequate, in scope and in quality, as a thesis for the degree of Master of Science.

_____

Assist. Prof. Dr. Mehmet Zeyyad Baykara (Advisor)

_____

Assist. Prof. Dr. Yegân Erdem

_____

Assoc. Prof. Dr. Erdem Alaca

Approved for the Graduate School of Engineering and Science:

_____

Prof. Dr. Levent Onural

Director of the Graduate School

ABSTRACT

NANOTRIBOLOGICAL PROPERTIES OF GRAPHENE GROWN BY CHEMICAL VAPOR DEPOSITION AND TRANSFERRED ONTO SILICON OXIDE SUBSTRATES

Tuna Demirbaş

M.S. in Mechanical Engineering

Advisor: Assist. Prof. Dr. Mehmet Zeyyad Baykara

October, 2015

To extend the lifespan of mechanical systems, wear and friction must be minimized with the utilization of lubricants. On the other hand, traditional fluid-based lubrication schemes fail in nano- and micro-scale systems due to increasing surface-to-volume ratios and associated physical effects. As such, research efforts in recent years have been aimed at characterizing the structure and mechanical properties of various candidates for solid lubricants.

Due to its outstanding electronic and mechanical properties, the *two-dimensional* "wonder material" graphene has been the focus of a large variety of experiments in the past decade. Based on its promise as a single-layer solid lubricant suitable for use in nano- and micro-scale systems, the nanotribological properties of graphene have been investigated in several studies in the literature. While frictional characteristics of mechanically exfoliated graphene samples as a function of layer number have been related to the effect of *puckering*, the nanotribological behavior of graphene samples grown by chemical vapor deposition (CVD) is still under investigation. Considering that high quality graphene of sufficient dimensions for practical applications is currently grown by CVD and requires transfer from metal foils onto various substrates, the need for an extensive understanding of the nanotribological properties of such graphene samples arises.

Based on the discussion above, this M.S. thesis presents a comprehensive structural and nanotribological characterization of CVD-grown graphene transferred onto oxidized silicon substrates (SiO_2/Si). In particular, the processes of sample preparation and post-preparation transfer onto SiO_2/Si substrates are optimized via a series of experiments. Advanced microscopy techniques are utilized for the structural and morphological characterization of the obtained graphene films. In particular, optical microscopy, scanning electron microscopy (SEM), and atomic force microscopy (AFM) are used to inspect graphene coverage on the substrate and associated structural features. On the other hand, Raman spectroscopy is employed to confirm the single-layer character of CVD-grown samples.

The nanotribological properties of CVD-grown graphene samples on SiO_2/Si are studied by AFM in the friction force microscopy (FFM) mode under ambient conditions by measuring the evolution of friction force with increasing normal load. The effect of using different probe tips, growth conditions, and post-transfer cleaning procedures on frictional behavior is evaluated. A comparison of lubrication performance with mechanically-exfoliated graphene is also performed. Results indicate that CVD-grown graphene acts as a very good solid lubricant on SiO_2/Si, reducing coefficients of friction by ~90% for all investigated samples. It is shown that as-transferred CVD-grown graphene exhibits the highest mean lubrication performance and that the associated values drop slightly with post-transfer cleaning. Finally, the effect of *wrinkles* associated with CVD-grown graphene on measured friction values are quantitatively evaluated, with results revealing a substantial increase in friction on these structural defects.

Keywords: Graphene, Nanotribology, Chemical vapor deposition, Atomic force microscopy, Friction force microscopy

ÖZET

KİMYASAL BUHAR BİRİKTİRME YÖNTEMİYLE BÜYÜTÜLEN VE SİLİSYUM OKSİT ALTTAŞ ÜZERİNE TRANSFER EDİLEN GRAFENİN NANOTRİBOLOJİK ÖZELLİKLERİ

Tuna Demirbaş

Makine Mühendisliği, Yüksek Lisans

Tez Danışmanı: Yrd. Doç. Dr. Mehmet Zeyyad Baykara

Ekim, 2015

Mekanik sistemlerin ömürlerini uzatmak amacıyla, sürtünme ve aşınma, kayganlaştırıcı malzeme kullanımı ile azaltılmalıdır. Öte yandan, artan yüzey-hacim oranları ve ilgili fiziksel etkiler sebebiyle, sıvı temelli geleneksel yağlama yaklaşımları, nano- ve mikro-boyutlu sistemler için başarılı olmamaktadır. Bu sebeple, geçtiğimiz yıllarda araştırma çalışmaları bir takım katı kayganlaştırıcı adayının yapısal ve mekanik karakterizasyonuna yönelmiştir.

Sahip olduğu sıra dışı elektronik ve mekanik özellikler sebebiyle, iki boyutlu "mucize malzeme" grafen, geçtiğimiz on yıl içerisinde birçok farklı deneyin hedefinde yer almıştır. Nano- ve mikro-boyutlu sistemlerde kullanıma uygun, tek katmanlı katı bir kayganlaştırıcı potansiyeli sergilemesi sebebiyle, grafenin nanotribolojik özellikleri literatürde bulunan bir grup çalışma vasıtasıyla incelenmiştir. Mekanik soyma yöntemi ile elde edilmiş grafenin katman sayısına bağlı sürtünme karakteristikleri *buruşma* etkisi ile ilişkilendirilmiş olsa da, kimyasal buhar biriktirme (KBB) yöntemi ile büyütülmüş grafen numunelerin nanotribolojik davranışı halen incelenmektedir. Pratik uygulamalar için yeterli boyuta sahip, yüksek kaliteli grafenin hâlihazırda KBB yöntemi ile büyütüldüğü ve metal folyolardan çeşitli alttaşlara transferinin gerektiği göz önüne alındığında, bu tarz grafen numunelerin nanotribolojik özelliklerinin etraflıca anlaşılmasına yönelik bir ihtiyaç ortaya çıkmaktadır.

Yukarıdaki tartışmadan yola çıkarak, bu yüksek lisans tezi, KBB ile büyütülmüş ve oksitlenmiş silisyum alttaşlara (SiO_2/Si) transfer edilmiş grafene yönelik kapsamlı bir yapısal ve nanotribolojik karakterizasyon çalışması sunmaktadır. Bilhassa, bir dizi deney vasıtasıyla, numune hazırlama ve ardından gerçekleşen SiO_2/Si üzerine transfer süreçleri en iyileştirilmiştir. Elde edilen grafen filmlerin yapısal ve morfolojik karakterizasyonu için ileri mikroskopi teknikleri kullanılmıştır. Özellikle, grafenin alttaş üzerindeki kapsama miktarı ve ilgili yapısal özellikler; optik mikroskopi, taramalı elektron mikroskopisi ve atomik kuvvet mikroskopisi (AKM) ile incelenmiştir. KBB ile büyütülmüş numunelerin tek-katman karakterini onaylamak amacıyla, Raman spektroskopisi kullanılmıştır.

KBB ile büyütülmüş grafen numunelerin SiO_2/Si üzerinde sergiledikleri nanotribolojik özellikler; sürtünme kuvvet mikroskopisi (SKM) modunda çalışan AKM ile ortam koşulları altında, sürtünme kuvvetinin artan normal yükle değişimini ölçerek belirlenmiştir. Değişik uç kullanımının, numune büyütme koşullarının ve transfer sonrası temizleme prosedürlerinin sürtünme davranışına olan etkileri değerlendirilmiştir. Bunun haricinde, mekanik soyma ile elde edilen grafen numunelerle kayganlaştırma performansına yönelik bir karşılaştırma da gerçekleştirilmiştir. Sonuçlar, incelenen tüm numuneler için, KBB ile büyütülmüş grafenin SiO_2/Si üzerinde çok iyi bir kayganlaştırıcı görevi gördüğünü ve sürtünme katsayısı değerlerini ~90% seviyesinde azalttığını göstermiştir. KBB ile büyütülmüş grafenin, transfer edilmiş haliyle en yüksek ortalama kayganlaştırma performansını sergilediği ve ilgili değerlerin transfer sonrası temizlemeyle ufak bir miktar düştüğü gösterilmektedir. Son olarak, KBB ile büyütülmüş grafende bulunan *kırışıkların* ölçülen sürtünme değerleri üzerine etkisi sayısal olarak değerlendirilmiş, sonuçlar bahsi geçen yapısal kusurlar üzerinde sürtünme değerlerinin önemli miktarda arttığını ortaya çıkarmıştır.

Anahtar Kelimeler: Grafen, Nanotriboloji, Kimyasal buhar biriktirme, Atomik kuvvet mikroskopisi, Sürtünme kuvvet mikroskopisi

Acknowledgement

First of all, I would like express my gratitude to my academic advisor, Prof. Mehmet Zeyyad Baykara, for his unending support and guidance which enabled me to finish my dissertation, as well as giving me an opportunity to be in his research group. Without his presence and knowledge I would have never been able to complete my research and this dissertation. He has been a great, caring, patient and creative professor who has taught me a lot.

Furthermore, I am deeply thankful to the Faculty of Engineering of Bilkent University and the National Nanotechnology Research Center (UNAM) administrators who provided an excellent scientific environment, as well as the necessary tools and materials for my studies. I will never forget all the technicians at UNAM who have always been kind to me. I have always valued their cooperation and kindness.

Additionally, I would also like to thank all my friends in the Scanning Probe Microscopy (SPM) research group: Arda Balkancı, Ebru Cihan, Tarek Abdelwahab, Alper Özoğul, Berkin Uluutku, Zeynep M. Süar and Verda Saygın for their friendship and contributions to my work. We have always motivated each other and worked well and hard in order to overcome any obstacles in research.

Last but not least, I can never thank enough my family for everything they did for me. Their support and caring helped me a lot throughout this hard and tough process. My mother, father and my grandmother have always been there for me. Without their endless love and support, I would not be able to make any significant progress in my work.

To my dear family

Contents

List of Figures

List of Tables

Chapter 1

Introduction

1.1 Overview

People who lived in ancient times came up with two outstanding discoveries which were, to a large extent, friction-related. For heating and cooking purposes, they used frictional heating achieved by rubbing two objects in rapid fashion, which is partially responsible for the discovery of fire. Additionally, they discovered that friction forces associated with rolling are generally smaller than those associated with sliding, a discovery that led, at least partially, to the invention of the wheel. From ancient to modern times, friction has had a vital impact in our daily lives: People would not be able to walk, drive, write, or even hold objects without the existence of the friction. On the other hand, excessive friction experienced by surfaces in contact leads to wear and causes dissipation of potentially useful energy via, e.g., generation of heat. On that account, it is desired to reduce friction in many practical applications and devices that feature sliding components, mostly via the use of suitable lubricants. In that context, graphene, a recently discovered *two-dimensional* material with numerous outstanding physical properties, possesses the potential to be an effective solid lubricant.

This M.S. thesis focuses on the preparation of graphene on copper foils via the method of *chemical vapor deposition* (CVD), as well as its structural and nanotribological

characterization using advanced microscopy techniques. In particular, *atomic force microscopy* (AFM) is employed to study the lubrication properties of CVD-grown graphene transferred onto oxidized silicon substrates (SiO_2/Si) as a function of normal load and post-transfer cleaning procedure. It is projected that the results presented in this thesis will further contribute to a complete physical understanding of frictional properties exhibited by two-dimensional materials and help evaluate graphene's potential as a solid lubricant in practical applications. In the following sections of this introductory chapter, the significance of friction, nanotribology, and graphene is briefly discussed and finally, an outline of the thesis is provided.

1.1.1 Friction: History and Importance

When an object (usually called the *slider*) slides on another object (usually called the *substrate*), its motion is typically opposed by a *friction force*. On the other hand, the force one needs to overcome to make an initially stationary object move on another object is also due to friction. As indicated in the previous section, friction is necessary to prevent slipping and sliding, and thus allows living creatures to be mobile in an efficient fashion. However, it induces energy dissipation which results in significant amounts of economic loss in industrial processes, most prominently in large-scale manufacturing. In various scenarios, friction can be minimized by using lubricants, reducing the weight of the associated objects, or by the use of rolling elements.

Friction has been the subject of a number of documented studies and investigations since hundreds of years. In the site of El-Bersheh, Egypt, a drawing dated 1880 B.C was discovered. This drawing shows a colossus being pulled on a sledge by a group of slaves, and a man (supposedly a mechanical engineer) pouring a liquid lubricant in front of the path of motion of the sledge to reduce frictional resistance to motion (Figure 1.1) [1].

A large number of scientists have worked on the concept of friction throughout history (Figure 1.2). Leonardo da Vinci (1452–1519), who has performed the first documented scientific studies related to friction and wear, has investigated friction force on horizontal and inclined planes, introduced the concept of the *coefficient of friction*, and the fact that friction does not depend on *apparent* contact area. Da Vinci

unfortunately has not published his work. In year 1979, Duncan Dowson presented Da Vinci's tribology work (including his notes and sketches on the subject) in his book titled "History of Tribology". On the other hand, more than hundred years after Da Vinci, Robert Hooke (1635–1703) studied rolling friction and focused specifically on the concept of adhesion [1]. A contemporary scientist with Robert Hooke, Guillaume Amontons (1663-1705), in 1699, rediscovered the first and second laws of friction which were discovered but not published by Da Vinci. Amontons' first law states that the friction force is directly proportional to the normal load and his second law indicates that the friction force does not depend on the apparent contact area [2]. Leonhard Euler (1707-1783) was the first man who has distinguished static and kinetic friction. Charles-Augustin de Coulomb (1736-1806) has introduced "Coulomb's Law of Friction" which emphasizes that kinetic friction is independent of the sliding velocity [3]. Additionally, Coulomb has analyzed the influence of the structure of contacting surfaces, the contact area, the normal load between the surfaces, and the elapsed time while the surfaces are in contact, on friction [1]. These observations led to the following common "law of friction":

$$\mu = F_f / F_n \qquad (1.1)$$

where μ is the *coefficient of the friction* (which is a constant that *only* depends on the type of materials in contact), F_f is the friction force, and F_n is the normal load [4].
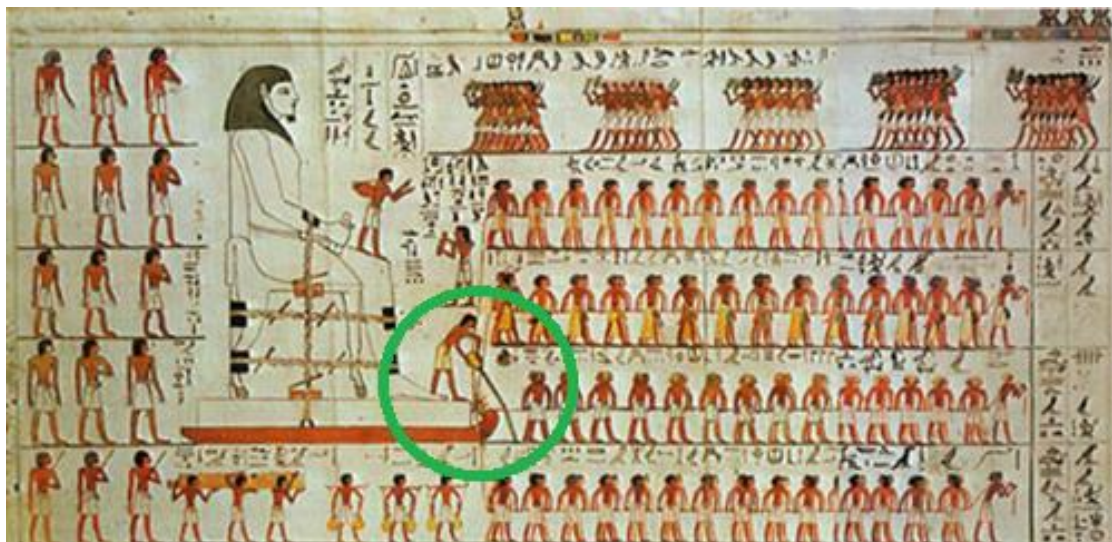
Figure 1.1 An Egyptian engineer using a liquid lubricant to aid the movement of a sledge carrying a large statue, in El-Bersheh, Egypt, in 1880 B.C [6].

Frank Philip Bowden (1903-1968) and David Tabor (1913- 2005) have later determined that the *actual* contact area between two objects is significantly less than the *apparent* contact area as the interface is of *multi-asperity* character, meaning that it is made up of numerous small regions of contact between the asperities of slider and substrate (Figure 1.2) [5]. This fact introduced a considerable difficulty to the correct physical interpretation of macroscopic friction experiments, as the *actual* contact area cannot be determined reliably in most practical scenarios. However, the research field of nanotribology, introduced more than two decades ago, has provided an elegant solution to this problem via the utilization of AFM, which will be discussed in the following section.
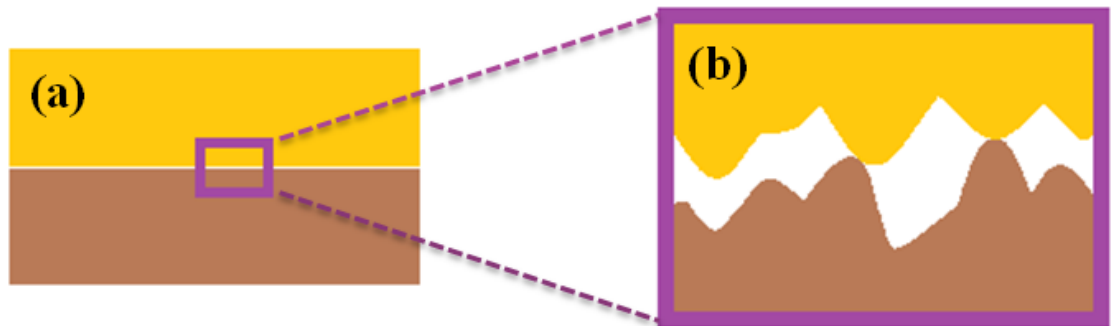
Figure 1.2 (a) A sketch demonstrating that the *apparent* contact area at the interface between two macroscopic objects appears reasonably flat. (b) The zoomed-in view of the interface which demonstrates that the actual contact between the two surfaces is of multi-asperity character.

1.1.2 Nanotribology: Searching for the Origins of Friction via Atomic Force Microscopy

Physicist Richard Feynman (1918-1988) is widely regarded as the father of *nanotechnology*, due to his well-known lecture titled "There is Plenty of Room at the Bottom" that he delivered at an APS meeting in CalTech in 1959. Several decades after the lecture by Feynman, nanoscience and nanotechnology have become subjects of intense scientific research and there are already a number of manufacturing methods, devices and other consumer goods on the market that rely on nano-scale components and phenomena. Within this context, it can be argued that the invention of scanning probe microscopy (SPM) methods including *scanning tunneling*

microscopy (STM) [7] and *atomic force microscopy* (AFM) [8] by Gerd Binnig *et al.* (which eventually led to the Nobel Prize in Physics in 1986 [9]) have been the main driving force behind nano-research, due to the capability that they provide in terms of very high (down to *atomic-scale*) resolution imaging and spectroscopy of surfaces.

The Greek word *tribos* which means "rubbing", is the origin of the word *tribology* coined by Peter Jost in 1966 [3]. Tribology is the study of interacting surfaces in relative motion; in other words, it is the "science of friction, wear, and lubrication". A prefix "nano" is added to the word tribology when the scale of the study descends to the order of nanometers (1-100nm). Over the past few decades, the research field of *nanotribology* has become an essential branch of nanoscience and nanotechnology.

As already discussed in the previous section, most surfaces are not perfectly (i.e., *atomically*) smooth on the nanoscale, leading to the so-called multi-asperity character. While certain characterization methods and tools such as the surface force apparatus (SFA) invented by J. N. Israelachvili and co-workers in the 1970s allow the precise measurement of friction forces acting between specific surfaces in relative motion [10], the invention of the AFM was instrumental in the progress of nanotribology, as the sharp AFM probe tip (curvature of radii typically below 100 nm) presents the opportunity to study friction acting at a *single asperity* (Figure 1.3) [11].

While the details of the AFM method for nanotribology research are discussed in Chapter 4, let us indicate that the basic operating principle relies on the detection of normal *and* lateral forces experienced by a very soft spring in the form of a micro-machined cantilever via a *laser beam deflection* (LBD) approach. As already indicated, the cantilever (which is typically fabricated out of Si, SiO_2 or Si_3N_4) is terminated by a sharp tip apex (the *single asperity*), which is brought into light contact (normal loads on the order of nN) with the sample surface to be investigated and raster-scanned with pm precision. The interaction of the probe tip with the surface in terms of normal and lateral forces are detected, which allows the study of friction (as inferred from lateral forces) as a function of sample material, normal load, etc., thus contributing remarkably to nanotribology research. For a comprehensive review of significant results achieved by the use of AFM in nanotribology research, the reader is directed to Ref. [12].
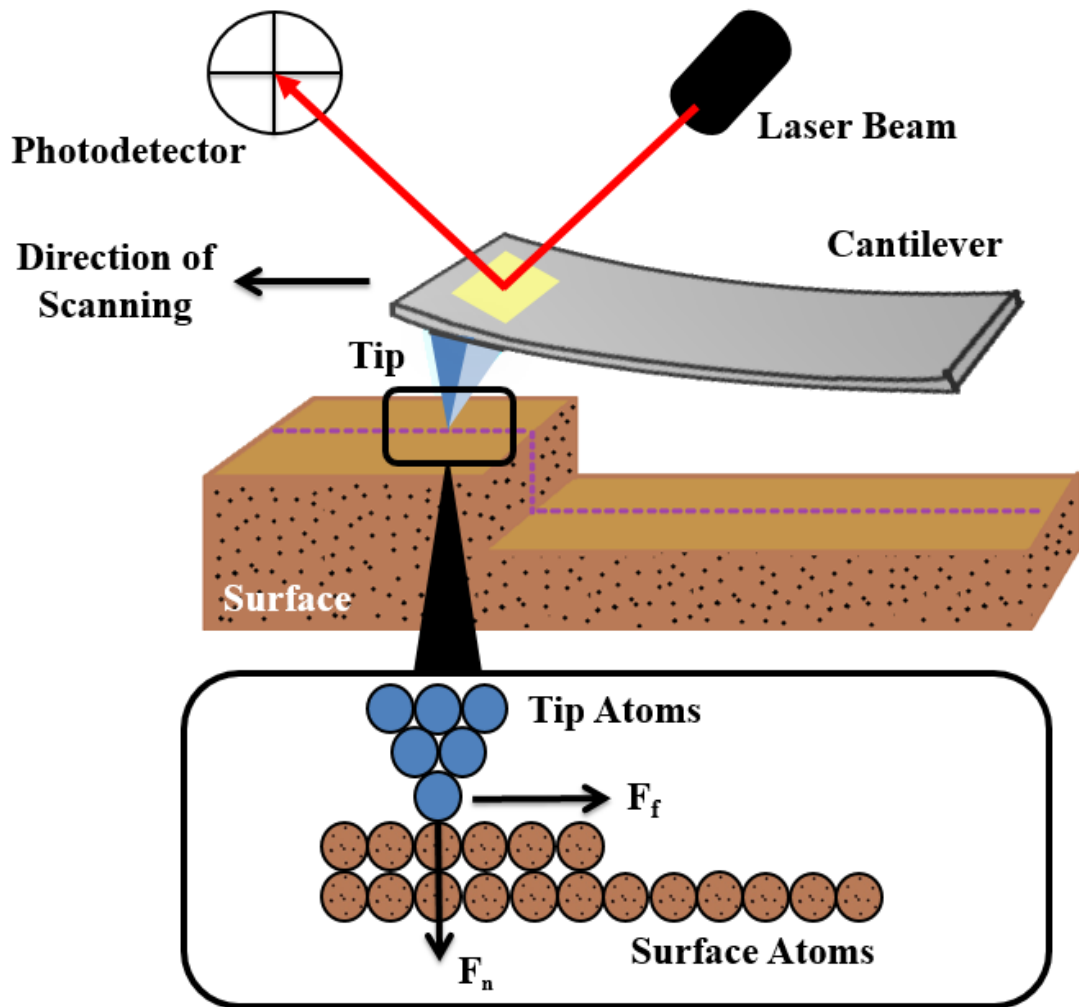
Figure 1.3 A schematic drawing of the fundamental elements of an AFM, and a representation of the single-asperity nature of the probe tip on the sample surface. Adapted from www.keysight.com.

1.1.3 Graphene: The "Wonder Material"

The word "graphene", coined by Hanns-Peter Boehm, originates from the combination of the word graphite and the suffix "–ene" [13]. Graphene is a *two-dimensional* material, in the sense that it is essentially a *single* sheet of carbon atoms arranged in a honeycomb lattice, which would in principle constitute a single layer of bulk highly oriented pyrolytic graphite (HOPG). Two researchers at the University of Manchester, Andre Geim and Konstantin Novoselov, have accomplished producing, identifying, and characterizing the physical properties of graphene as reported by a series of papers starting in 2004 [14, 15], which eventually

led to the awarding of the Nobel Prize in Physics in the year 2010. The prize winning graphene was fabricated by the so-called mechanical exfoliation method, where a bulk HOPG sample is peeled off by ordinary scotch tape, and made repeatedly thinner by folding the tape over itself, with the eventual attachment of single- and few-layer graphene samples to a target substrate (typically SiO_2/Si) [14, 15].

Graphene arouses interest both theoretically and experimentally due to its exceptional physical properties [16]. This remarkable material is an allotrope of carbon that consists of sp^2-bonded carbon atoms in a two-dimensional honeycomb lattice where the interatomic distance between the carbon atoms is 0.142 nm (Figure 1.4).

0.142 nm
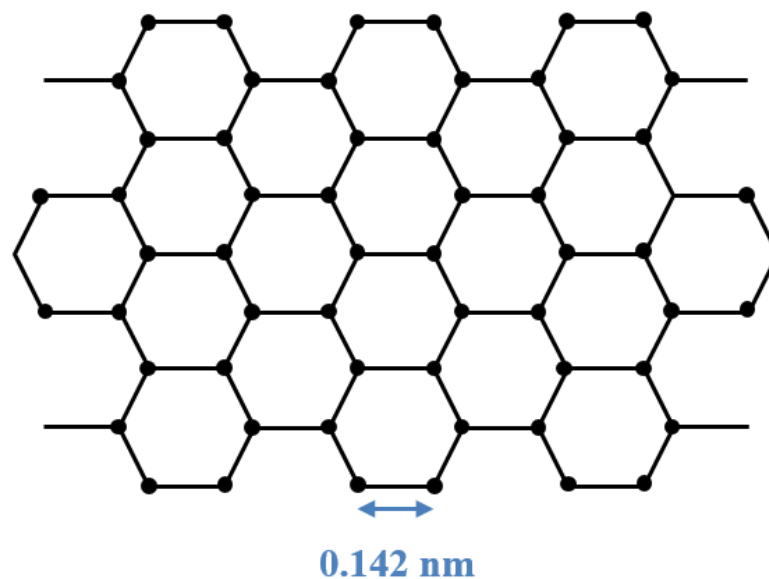
Figure 1.4 The structure of graphene.

Among the many interesting properties of graphene, its electrical and mechanical characteristics are of particular importance. Specifically, graphene has a peculiar band structure that results in its behavior as a "zero bandgap two-dimensional semiconductor" where electrons are considered to be *massless* Dirac fermions [17]. This leads to high electron mobilities of ~10,000 $cm^2/V \cdot s$ observed at room temperature for exfoliated graphene samples [15]. On the other hand, pioneering AFM experiments conducted on exfoliated graphene have revealed outstanding mechanical properties associated with this material, namely a Young's modulus value of ~1.0 TPa and an intrinsic strength of ~130 GPa, at which fracture occurs [18]. The frictional properties of graphene have also been investigated in a relatively small number of

publications over the last decade (e.g., Ref. [19, 20]). An overview of related results and how the work presented in this thesis complements the studies in the literature is provided in Chapter 4.

Finally, it should be indicated that in addition to mechanical exfoliation, graphene can be obtained by *chemical vapor deposition* (CVD) on metal surfaces such as copper [21], as well as *epitaxial growth* on silicon carbide (SiC) [22]. While each method and the resulting graphene samples have advantages and disadvantages for various applications, the CVD method has been preferred to produce the graphene samples investigated nanotribologically in this thesis, based on the fact that the CVD approach provides single-layer graphene samples on the length scale of centimeters (whereas single-layer graphene flakes produced by mechanical exfoliation are rarely larger than 100 μm). As the main aim of the work presented here is to evaluate the lubrication properties of graphene sheets in sizes that would be potentially useful for practical applications, the CVD method has been employed to produce the samples.

1.2 Outline

In this introductory chapter (Chapter 1), the history and importance of friction have been emphasized, and the research field of nanotribology as well as the "wonder material" graphene have been introduced. The chapter underlines that this M.S. thesis is devoted to the nanotribological characterization of CVD-grown graphene via AFM and an evaluation of its potential as a solid lubricant.

In Chapter 2; the preparation, transfer, and post-transfer cleaning procedures associated with CVD-grown graphene are described. The chapter also includes a brief literature review of the CVD process for graphene growth.

Chapter 3 reports the results of the structural and morphological characterization of CVD-grown graphene, as conducted by optical microscopy, Raman spectroscopy, scanning electron microscopy, and atomic force microscopy. The obtained data highlight that single layer graphene sheets of sufficient size are synthesized successfully.

Chapter 4 titled "Nanotribological Characterization of CVD-Grown Graphene Transferred onto SiO_2/Si Substrates" forms the main part of this M.S. thesis. In this chapter, the basic operating principle of AFM and the associated force calibration procedures are described first. Subsequently, results of AFM-based nanotribology measurements on CVD-grown graphene are presented. The dependence of friction on normal load is examined in detail. Additionally, the effects of using different tips, employing different growth conditions and performing different post-transfer cleaning procedures on observed friction force values are reported. The chapter includes an overall evaluation of the lubrication performance of CVD-grown graphene on SiO_2/Si.

Finally, Chapter 5 provides a general summary of the experimental study presented in the thesis, as well as an outlook regarding future research directions.

Chapter 2

Sample Preparation: Chemical Vapor Deposition, Transfer onto SiO₂/Si Substrates, and Post-Transfer Cleaning

2.1 Background

As indicated earlier, the two-dimensional material graphene with its outstanding physical properties has received tremendous attention globally and has recently become one of the so-called *hot* topics of nano-scale scientific research. One of the main thrusts of graphene research has been placed on gaining the capability to produce single-layer samples on large scales (centimeter-scale and above), while minimizing defect formation. Among various techniques that have been proposed and applied for the production of graphene, the *chemical vapor deposition* (CVD) method has been so far the most successful in terms of obtaining large-scale graphene samples with single layer character. While the procedural details of the CVD approach to graphene growth are reported in Section 2.2, a brief review of related scientific efforts in the literature is given below.

In the year 2006, Somani *et al.* wrote the first report related to synthesis of few-layer graphene on nickel substrates via the pyrolysis of camphor, utilizing a CVD-based approach [23]. The first study involving single- to few-layer graphene growth via

CVD of methane (CH_4) on polycrystalline nickel films, and the subsequent transfer of the resulting material to arbitrary substrates such as SiO_2/Si (i.e., an oxidized Si wafer) was realized by Reina et al. [24]. Shortly after the mentioned work, the synthesis of high quality and large-scale graphene with uniform *single-layer* character was achieved by X. Li *et al.* via the CVD of CH_4 on a 25 μm thick copper foil [21]. Following the demonstration of the CVD growth of single- and few-layer graphene on copper and nickel foils, CVD growth of graphene on a 25 μm thick gold substrate has been reported by the group of C. Kocabaş at Bilkent University [25]. The common aspect of the substrates used in the reported studies (Cu, Ni, Au) is chemical in character such that they are all transition metals. In the growth process, the transition metal surfaces act as catalysts for the decomposition of carbon-carrying gases (such as methane) such that carbon atoms are accumulated on the surfaces, eventually forming graphene [26].

After graphene growth via CVD on transition metal surfaces such as copper, it is typically desired to transfer graphene from the metal surface to a target substrate (such as SiO_2/Si) for potential use in various applications. However, transfer procedures associated with graphene are quite challenging, mainly due to the occurrence of structural damage (such as the formation of *tears* and *folds*) and potential contamination (due to the chemicals involved in the process) during the transfer. The considerable lateral sizes of graphene sheets grown via CVD also cause practical problems associated with transfer to a new substrate. The transfer procedure associated with CVD-grown graphene typically involves a polymer *handle layer* such as poly (methyl methacrylate) PMMA [27, 28, 29], poly (dimethylsiloxane) PDMS [30], thermal release tape [31], self-release layer (SRL) [32], or poly (bisphenol A carbonate) PC [33]. Among these, the PMMA-based transfer method is the most commonly used, mainly due to its procedural simplicity. PMMA, which is used as a sacrificial handle layer in the transfer process, inevitably leaves a certain amount of chemical residue on the graphene samples after transfer to different substrates. In order to clean the chemical residue on graphene, post-transfer cleaning steps can be employed. There are several cleaning procedures practiced in the literature, as further explained in Section 2.4.

This chapter is devoted to the procedural details associated with the preparation of graphene samples (in particular; CVD growth, transfer, and post-transfer cleaning), the nanotribological properties of which are subsequently analyzed via AFM as reported in Chapter 4.

2.2 Graphene Growth on Copper Foils via CVD

2.2.1 Basic Principle of the CVD Process

The *chemical vapor deposition* (CVD) process is a common bottom-up microfabrication method used for producing thin films (chiefly in the semiconductor industry), involving the deposition and subsequent decomposition of gaseous precursors on a substrate which is typically held at elevated temperatures to facilitate the involved chemical reactions. There are plenty of variations of CVD; foremost among them are atmospheric pressure CVD (APCVD), low pressure CVD (LPCVD), and ultrahigh vacuum CVD (UHVCVD). APCVD operates at atmospheric pressure, LPCVD works at under sub-atmospheric pressures and UHVCVD is functional at extremely low pressures ($\sim 10^{-8}$ mbar or lower) [34].
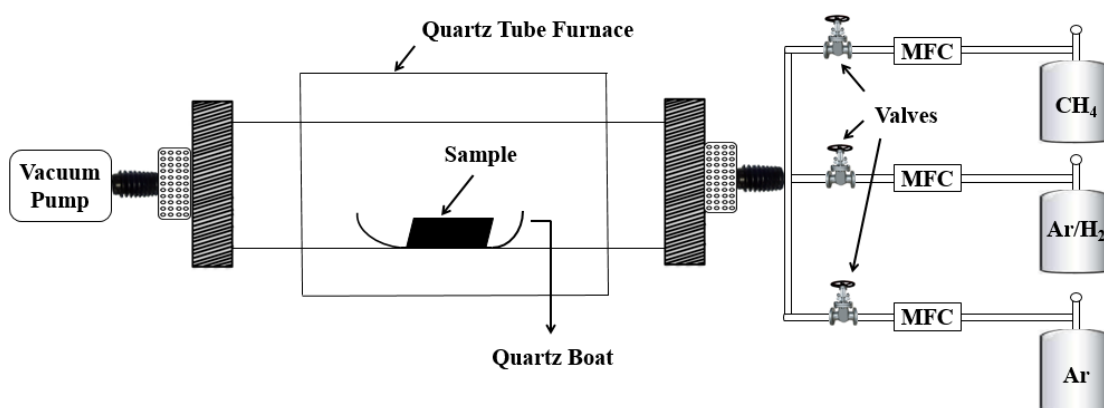
Figure 2.1 A schematic diagram of a typical CVD system based on a quartz tube furnace.

A typical CVD system is composed of a *furnace* that acts as the reaction chamber and the source of thermal energy as well as the manifold system for the delivery of the precursor/carrier gases to the reaction chamber, a vacuum pump for the removal of by-products in the form of unwanted gases, and process control equipment such as

mass flow controllers (MFCs) and valves (Figure 2.1). A picture of the CVD system used for the experiments reported in this M.S. thesis is provided in Figure 2.2.

Figure 2.2 A picture of the CVD system at the National Nanotechnology Research Center (UNAM) used for the experiments reported in thesis.

The sequence of the steps in a typical CVD process starts with the transport of the precursor gases to the heated reaction chamber and adsorption of these gases on the substrate surface. The process continues with the surface diffusion of precursor gases to the growth sites, chemical reactions leading to decomposition and eventual deposition of the resulting material on the substrate surface, accompanied by the desorption of gaseous by-products. As already indicated, the disposal of the gaseous by-products from the reaction chamber is usually performed by a vacuum pump. At the end of the process, the substrate is coated with a thin film of the desired material. It should be noted that the chemical reaction to break the bonds within the precursor gases is provided by the heat from the resistive elements in the furnace. The sample surface acts as a catalyst, reducing the energy barriers required for decomposition. The gases that are used in the process must be volatile and stable so as to be able to reach the reaction chamber and react with the substrate. As already indicated, the CVD approach is the preferred method for graphene production in this M.S. thesis, mainly due to the large size of the resulting samples.

2.2.2 Graphene Growth via CVD: Choice of Substrate

As a first step in the CVD process, the selection of the transition metal which is to be used as the substrate must be performed. In the literature, copper and nickel foils are widely used as catalysts for the CVD process. Due to significant differences in the solubility of carbon in the two materials, the growth mechanism differentiates for copper and nickel substrates. The solubility of carbon in copper is two orders of magnitude smaller than nickel (0.001% vs. 0.1%). This leads to the fact that CVD-growth on copper performed via methane at elevated temperatures (near 1000 $^{\circ}$C) results in almost uniform coverage of the substrate by single-layer graphene, while graphene grown on nickel features a large amount of multi-layer regions, caused by the precipitation of excess carbon in bulk Ni upon cooling of the foils due to the associated decrease in carbon solubility [35].

As a substrate for the growth of single-layer graphene samples, 25 μm thick copper foil with 99.8% purity (*Alfa Aesar*, product no. 13382) has been chosen, in accordance with reports in the literature [21]. The foil is cut in dimensions of 35 mm × 50 mm to be placed in quartz boats acting as carriers in the quartz tube furnace used for graphene synthesis.

It has been observed that the surface morphology and cleanliness of the copper foil significantly affect the quality of CVD-grown graphene. As such, a cleaning process is performed on the copper foils, with the intention of improving graphene quality by reducing surface roughness and removing organic impurities on the surface of the copper foil. The cleaning procedure begins by dipping the copper foils in acetone to remove organic impurities on the surface. However, as the evaporation rate of the acetone is very high, it leaves certain residues on the surface, which are removed in the second step of the cleaning procedure by isopropanol. In the next step, a diluted acid solution is prepared with 10 ml HCl and 90 ml double-distilled water. The copper foil is sunk into this solution for 5 minutes. Immersion into a double-distilled water bath follows the previous step to remove acid residues. Finally, the foil is dried with a nitrogen gun.
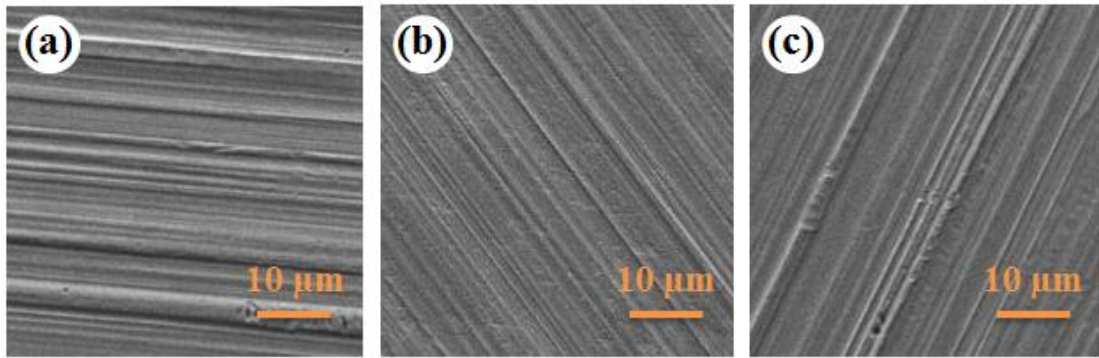
Figure 2.3 SEM images of the (a) as-received copper foil; (b) copper foil cleaned with diluted HCl acid solution, and (c) copper foil cleaned with diluted acetic acid solution.

To compare the effectiveness of the HCl acid in the context of foil preparation with another strong acid, acetic acid has been utilized. In Figure 2.3, SEM images of as-received copper foils, as well as those treated with HCl and acetic acid can be seen. In terms of surface morphology, it is observed that the as-received copper foil features the roughest texture, while the foil cleaned with HCl has the smoothest surface. Accordingly, the use of HCl acid solution in the treatment of Cu foils has been preferred in CVD experiments.

2.2.3 Graphene Growth via CVD: Experimental Procedure

For the experiments reported in this thesis, CVD growth has been performed using the system depicted in Figure 2.2, consisting of a quartz tube furnace (Protherm/AlserTeknik), a digital temperature controller (Honeywell DC1020), a vacuum pump (Varian DS202), and mass flow controllers (HoribaStec SECE40). The gas manifold attached to the gas cylinders and including various valves has been built using 316L stainless steel pipes. As oxygen leakage from the air causes oxidation of the copper foil at elevated temperatures and thus inhibits CVD growth, potential gas leaks have been regularly checked via helium leakage tests conducted with a standard instrument (Pfeiffer Vacuum Smart Test HLT570).

The first step in the CVD processes involves placing the copper foil prepared as in Section 2.2.2 into a quartz boat which is then loaded into the quartz tube furnace. The copper foil in its initial form typically features a thin oxide layer on top of its surface despite the cleaning steps discussed previously. The existence of this oxide layer is

detrimental for graphene growth as it leads to a reduction in catalytic activity. Therefore thermal annealing is applied on the copper foil in the presence of a reductive element such as hydrogen to get rid of the oxide layer. This process involves heating the furnace to 1000°C, and flowing of a mixture of H_2 and Ar gases (ratio 5:95) at 200 sccm (standard cubic centimeters per minute) for 30 minutes over the Cu foil. The thermal annealing process also increases the average grain size on the copper foil surface and thus reduces the negative effect of grain boundaries on the morphology of CVD-grown graphene [36]. SEM images of thermally annealed copper foils are provided in Figure 2.4 for reference.
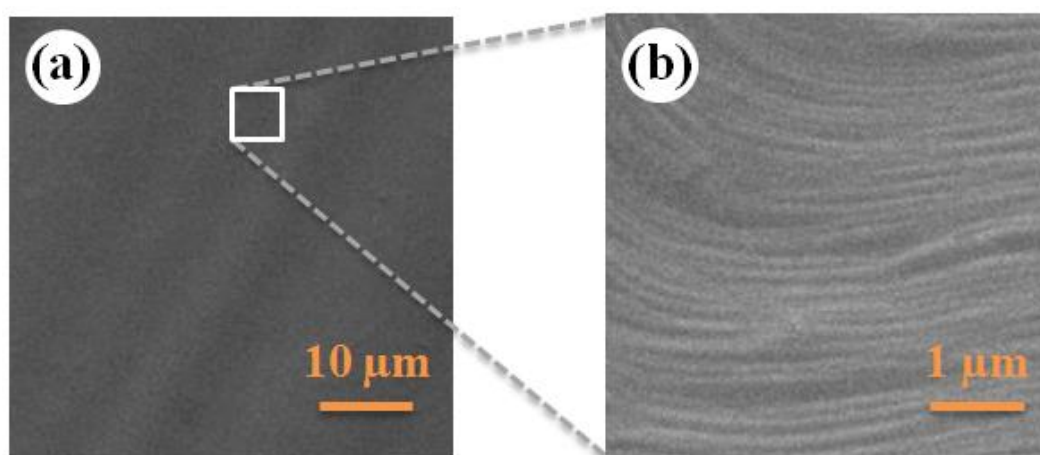
Figure 2.4 (a) SEM image of thermally-annealed copper foil. (b) Zoomed-in view of the marked portion, showing terraces separated by steps.

After thermally annealing the Cu foil, graphene growth is initiated with the introduction of CH_4 into the quartz tube, typically at 25 sccm. As already discussed, CH_4 is the source of carbon atoms which act as the building blocks of graphene on copper. The gas valves are closed and the furnace heating system is turned off after 20 minutes of CH_4 flow. The cover of the furnace is opened to increase cool-down rates. When room temperature is reached in the furnace, the vacuum pump is turned off and the sample is taken out of the quartz tube. The clearly observable difference in the appearance of the copper foils before and after the CVD process due to coverage by graphene is depicted in Figure 2.5.
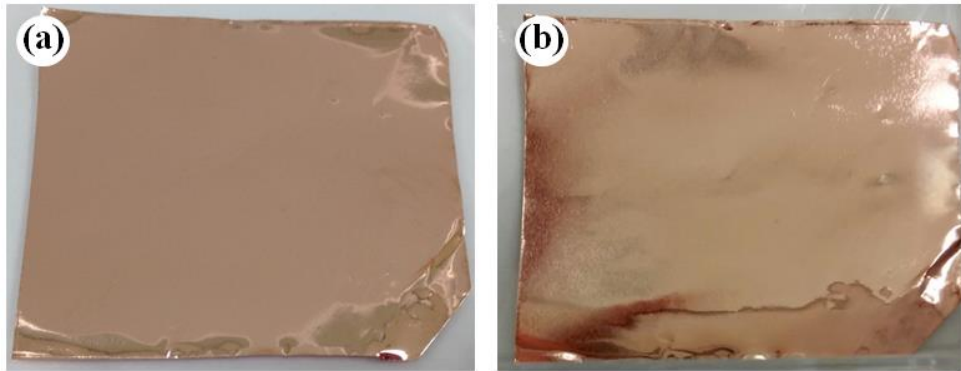
Figure 2.5 Copper foils (a) before, and (b) after graphene growth.

To obtain high quality graphene via CVD, it is important to optimize growth parameters, including temperature, flow rate and flow time of precursor and carrier gases. Due to the large number of involved parameters, lots of variations need to be tested to arrive at optimum conditions. For instance, two different approaches involving either (i) the simultaneous flow Ar/H_2 mixture and CH_4 or (ii) the flow of CH_4 only during graphene growth can be applied. A comparison of the quality of graphene grown via different combinations of experimental parameters is provided in Chapter 3.

2.3 Transfer of CVD-Grown Graphene onto SiO₂/Si Substrates

Once graphene is grown via CVD, it is typically desired to transfer it from the copper foil to an insulating surface for, e.g., electronic applications. Silicon wafers covered with silicon dioxide (SiO_2/Si) are traditionally preferred towards this purpose, as it has been shown that single- and few-layer graphene is optically observable on Si wafers covered with ~300 nm SiO_2 using a regular microscope [14].

In order to obtain clean graphene samples on SiO_2/Si samples, the level of contamination in the environment must be very low during the transfer. As such, the whole transfer procedure has been performed in the cleanroom facility of the National Nanotechnology Research Center (UNAM) for the experiments reported here. The concentration of airborne particles in the cleanroom is greatly reduced by

high-efficiency particulate air (HEPA) filters [37], providing optimum conditions for graphene transfer.

A sacrificial layer of poly (methyl methacrylate) (PMMA) with the chemical formula of $(C_5O_2H_8)_n$ has been used to support (i.e., hold) the CVD-grown graphene during the transfer process. As the first step of the transfer procedure, the copper foil covered with graphene is put onto a spin-coater and 5 droplets of PMMA 950 A2 are dropped onto it. The duration of spinning and the number of revolutions per minute are adjusted as 50 seconds and 4000 rpm, respectively. After the spin coating procedure, the sample is cured on a 110°C hot plate for 15 seconds. The sample is then cut according to the dimensions of the SiO_2 wafer (10 mm × 10mm), and is straightened with the aid of clean, flat handles of a pair of tweezers.

Next, a diluted nitric acid (HNO_3) solution is prepared by 5 ml nitric acid and 15 ml distilled water. In the quartz tube furnace, graphene coats both sides of the copper. First, graphene on the side of the foil not covered by PMMA must be etched away via HNO_3 in order to etch the copper beneath it. The HNO_3 solution etches the graphene in ~3 minutes and etching becomes apparent by the rising of plenty of bubbles to the surface of the solution. It is important in this step to make sure that the top surface of the foil (covered with PMMA) does not come into contact the solution. After the graphene etching process, the sample is dipped into distilled water to get rid of the residues associated with the HNO_3 solution.

To etch the copper foil away, a 1 M solution of ammonium persulfate $[(NH_4)_2S_2O_8]$ is prepared and put on a hot plate at 70 ^{o}C [38]. Consequently, the copper foil is placed on the solution. The duration of the copper etching process is approximately 20 minutes. The colorless solution gradually becomes blue as the copper is etched away. What remains behind is CVD-grown graphene, coated by PMMA.

Subsequently, SiO_2/Si wafers are cleaned ultrasonically in baths of acetone, isopropanol and distilled water. One wafer piece with relatively large dimensions is used as a handling tool and another one is used as the substrate. The larger SiO_2 wafer is utilized to *fish* the PMMA-covered graphene sample from the copper etchant solution and to place it in a beaker of distilled water in order to remove chemical residues associated with the etching process. Afterwards, the PMMA-covered

graphene sample is placed on the substrate SiO$_2$/Si wafer directly from the distilled water. Attention must be paid in this step to avoid excessive structural damage to graphene. Finally, to remove the PMMA support on graphene, the wafer is placed into acetone for 5 minutes. The whole transfer procedure is visualized in Figure 2.6.
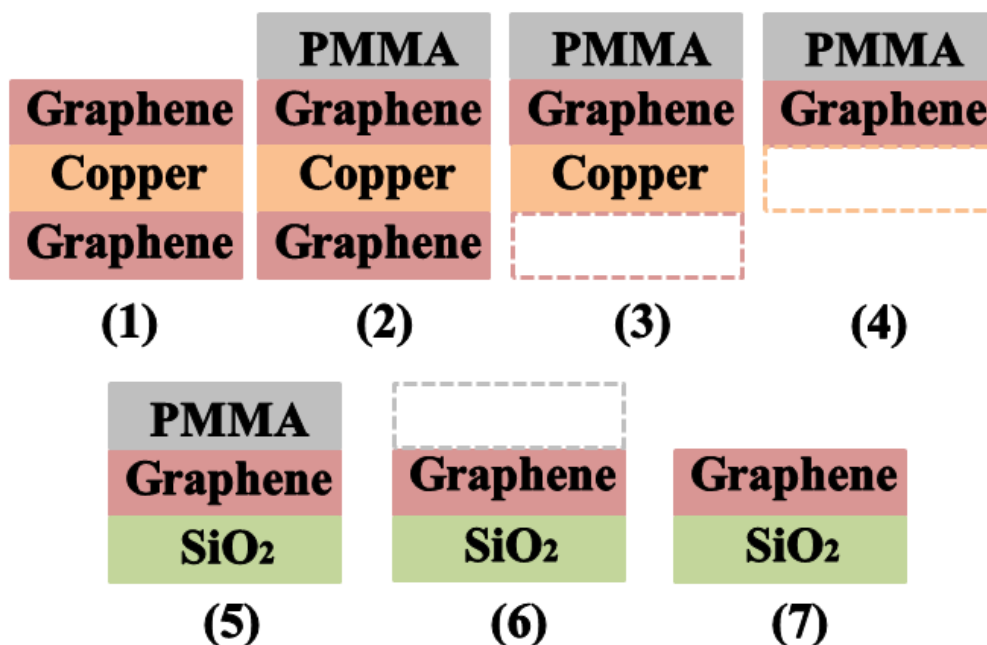
Figure 2.6 The process flow associated with the transfer of CVD-grown graphene onto silicon oxide substrates. Please note that the relative thickness of the layers is not in scale.

2.4 Post-Transfer Cleaning

As indicated in the previous section, PMMA serves as a supporting layer for graphene in the transfer process. Placing the PMMA-graphene stack in acetone is often not sufficient to remove the whole PMMA layer from graphene – residues are commonly observed, even with optical microscopy. Instead of using acetone as a solvent, dipping the sample into glacial acetic acid for 24 hours and then cleaning it in a methanol solution has been proposed as a way of dissolving PMMA better than acetone [39].

On the other hand, thermal annealing procedures have been also suggested to obtain clean graphene samples with minimal PMMA residues. In the literature, a wide range of thermal annealing procedures have been studied. Graphene samples contaminated

by chemical residues have been annealed in vacuum [40] as well as in the presence of Ar [27], Ar/H_2 [41], CO_2 [42], and N_2 [43] gases. Even under harsh conditions involving high temperatures and extended annealing times, the residuals of PMMA are never entirely removed from the graphene surface [44].

One of the aims of this thesis is to investigate the effect of different post-transfer cleaning procedures (see the two sections below) involving ultrasonic cleaning in acetone and isopropanol, as well as annealing under Ar gas, on the structural and nanotribological properties of graphene. The related results are presented in Chapter 3 and Chapter 4, respectively.

2.4.1 Ultrasonic Cleaning

Ultrasonic cleaning in various solvents is known to be effective in removing contaminants from various sample surfaces. The main working principle of the process is based on agitation of the cleaning medium (the solvent) via ultrasonic excitation to form cavitation bubbles on the surface of the object to be cleaned. Ultrasonic cleaning takes place in a tank containing the solvent, to which an ultrasonic transducer is attached. In this thesis, we evaluated the effect of post-transfer ultrasonic cleaning on the structural and nanotribological properties of CVD-grown graphene. Accordingly, the SiO_2/Si wafer covered with graphene is placed into a beaker containing acetone, which is then inserted in the tank of the cleaner. Next, the sample is cleaned in the ultrasonic cleaner for 20 seconds. Subsequently, the same treatment is applied to the sample in isopropanol. Finally, the sample is dried with nitrogen gas.

2.4.2 Annealing under Argon Flow

Motivated by attempts at removing PMMA residues via annealing under vacuum and Ar gas as reported in the literature [27, 40], we have evaluated the effect of thermal annealing under Ar flow on the structural and nanotribological properties of CVD-grown graphene. Towards this purpose, the SiO_2/Si wafer covered with graphene has been annealed in the quartz tube furnace, post-transfer, under Ar gas flow at 300°C for 2 hours.

Chapter 3

Structural and Morphological Characterization of CVD-Grown Graphene

3.1 Background

In Chapter 2, the procedural details associated with the growth, transfer, and optional post-transfer cleaning of graphene obtained by the CVD method have been described. On the other hand, before a comprehensive nanotribological characterization of CVD-grown graphene transferred onto SiO_2/Si substrates can be accomplished, the structural and morphological properties of the material in question should be investigated in detail.

Since the demonstration that graphene can be readily obtained by mechanical exfoliation about a decade ago, a diverse range of characterization tools including optical microscopy [14], Raman spectroscopy [45], scanning electron microscopy (SEM) [21], and atomic force microscopy (AFM) [46] have been employed to characterize the structural and morphological properties of graphene samples obtained via various means. In particular, such studies targeted a precise determination of the number of layers of graphene, its distribution and coverage on various substrates, as

well as a characterization of associated structural defects including but not limited to wrinkles, tears, and folds.

In this chapter, in line with the available literature on the subject, results of structural and morphological characterization studies on CVD-grown graphene films performed via optical microscopy, Raman spectroscopy, SEM, and AFM are presented; preceded by a brief overview of each method. The data discussed here demonstrates that single-layer graphene samples are successfully obtained via the approach presented in Chapter 2, and a detailed characterization of associated defects and contaminants is possible by employing the experimental techniques mentioned above.

3.1.1 Optical Microscopy and Graphene

When investigating the physical properties of any material, the first step involves macroscopic observation by naked eye, such that a rough idea about the structural and optical properties of the material is obtained. Obviously, the human eye is a limited observation tool for detailed scientific studies, due to its inability to discern micro-scale structural features. However, as it has been known for centuries, the sense of sight can be extended by optical instruments. In modern science, to study microscopic structural properties, an optical microscope can be used. A typical optical microscope illuminates the sample in question with visible light, and utilizes a system of lenses to obtain a magnified two dimensional image (Figure 3.1).

In the late 16th century Zacharias Jansen (1580-1638) invented a compound optical microscope with two lenses. The objective lens displays a primary, magnified image, and the second lens called the *eyepiece* is utilized for further magnification of the primary image [47]. Robert Hooke (1635-1703) improved the instrument by adding useful components such as a stage for holding the studied sample, coarse and fine focus control units for lateral and vertical positioning during imaging, and a dedicated illuminator. Perhaps more importantly, Carl Zeiss (1816-1888) and Ernst Abbe (1840-1905) enhanced the resolution of the optical microscope by (i) utilizing a condenser lens which concentrates light from the light source onto the sample and (ii) using lenses with superior optical quality (which mainly involves reduced surface roughness) [48].
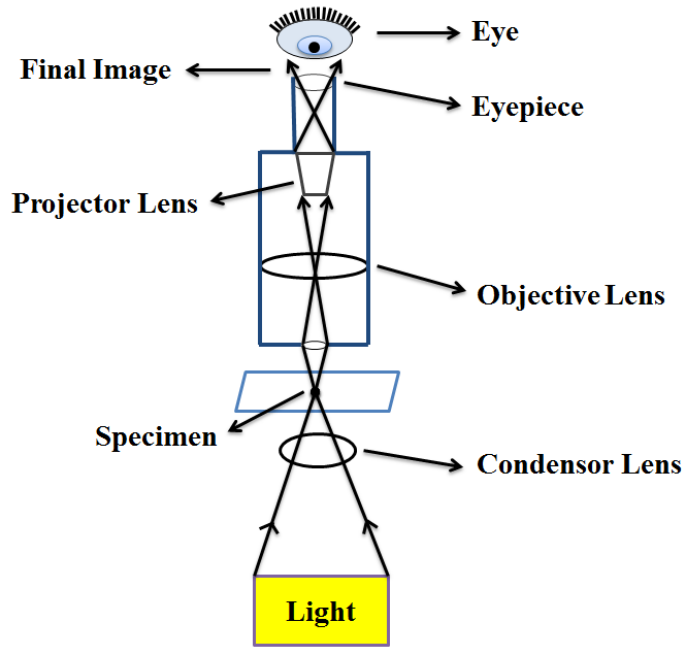
Figure 3.1 A schematic diagram of a typical, compound optical microscope.
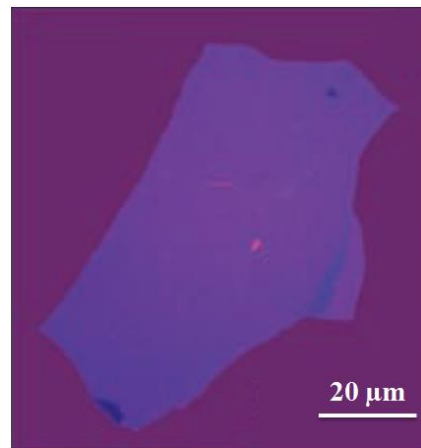
Figure 3.2 An optical microscopy image of mechanically-exfoliated graphene [14].

In one of their landmark papers describing the physical properties of mechanically exfoliated graphene, Novoselov *et al*. demonstrated that single-layer graphene, which is transparent to visible light, can be detected via optical microscopy (due to the increase in the optical path of visible light induced by the presence of the graphene) when placed on an oxidized Si wafer (SiO_2/Si) where the thickness of the oxide is ~300 nm [14]. In Figure 3.2, a representative optical microscope image of a mechanically-exfoliated graphene sample can be seen.

3.1.2 Raman Spectroscopy and Graphene

Raman spectroscopy is a widely-employed method which is used towards the chemical identification of various materials. The basic operating principle of Raman spectroscopy is based on the following: Monochromatic light from a laser source is used to illuminate the sample under investigation. As the laser light interacts with the sample, most of the photons are elastically scattered with no loss of energy, which constitutes Rayleigh scattering. However, a smaller amount of incident photons are inelastically scattered (due to interactions with the *phonons* of the sample), such that their energy either increases or decreases upon interacting with the sample, which is referred to as Raman scattering. By detecting the energy shift associated with scattered photons, which is unique for different materials, detailed chemical identification can be performed [49].
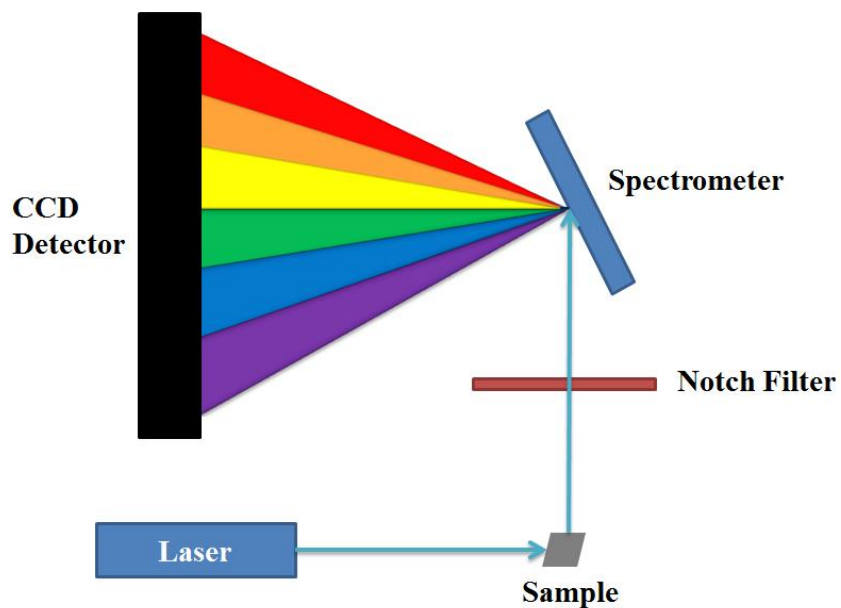
Figure 3.3 The basic functional components of a Raman microscope.

A typical Raman spectroscopy system has three main components, which are: (i) a monochromatic laser used as the excitation source, (ii) a notch filter, and (iii) a spectrometer with a charge coupled device (CCD) detector. The notch filter blocks scattered light with the exact wavelength of the excitation laser such that only energy-shifted (inelastically scattered) photons enter the spectrometer. The spectrometer with the CCD detector is used to detect the intensities associated with a

narrow region of wavelengths around the wavelength of the excitation laser (Figure 3.3).

The Raman effect described above has been discovered in year 1928 by Sir Chandrasekhara Venkata Raman (1888-1970). Consequently, in 1930, he was awarded with the Nobel Prize in Physics [50]. Interestingly, he actually utilized sunlight as an excitation source for his pioneering experiments, since the first laser was developed by Theodore Harold Maiman (1927-2007) only in 1960 [51].
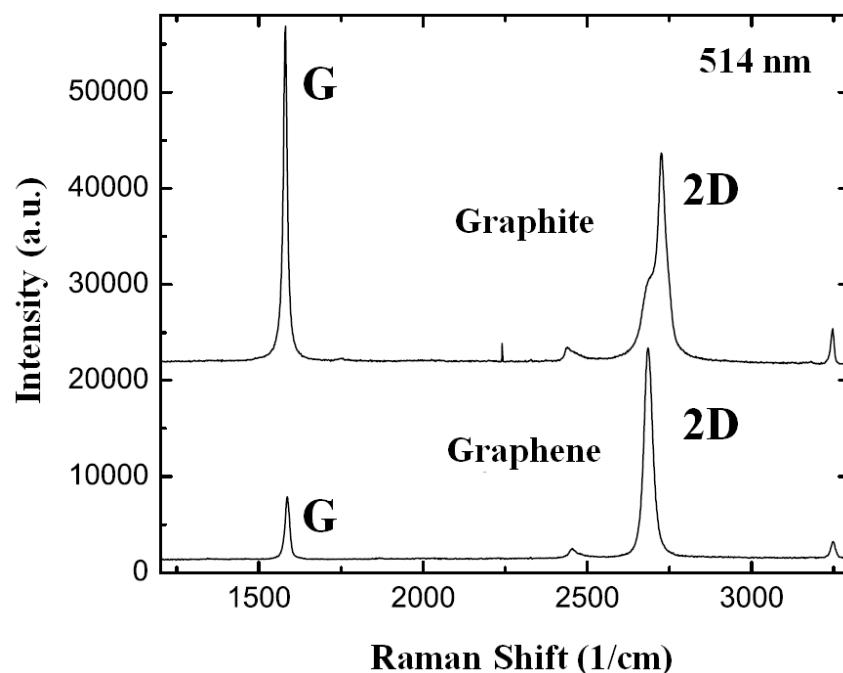
Figure 3.4 Comparative Raman spectra of graphite and mechanically-exfoliated, single-layer graphene, obtained with a monochromatic (514 nm) laser source [45].

Shortly after the demonstration that graphene can be readily obtained by mechanical exfoliation of graphite by Novoselov *et al.* [14], Raman spectroscopy has been employed to characterize its structure and chemistry by Ferrari *et al.* [45]. Specifically it has been shown that the number of layers of graphene samples can be precisely determined by such an approach [45]. The Raman spectrum of graphene features three main peaks which are referred to as the D, G, and 2D peaks. The positions of the D, G, and 2D peaks are approximately 1350 cm^{-1}, 1580 cm^{-1}, and 2700 cm^{-1}, respectively [45]. The D peak appears due to structural defects associated with graphene, such that in an ideal graphene sample the D peak should not be detectable. It has been shown by

Ferrari *et al.* that the relative intensities of the 2D peak and G peak (I_{2D}/I_G, or simply $I_{2D/G}$) can be utilized in the differentiation of single-layer, bi-layer, and multi-layer graphene samples, such that $I_{2D/G}$ ratios of ≥ 2, ~1, and <1, are typically expected for each case, respectively. Figure 3.4 shows the classic Raman spectra obtained by Ferrari *et al.* on bulk graphite, as well as a single-layer, mechanically-exfoliated graphene sample. Note that, in addition to the $I_{2D/G}$ ratio, variations in the shape of the 2D peak as well as its Raman shift value may be used as identifiers to distinguish single-layer graphene samples from bi-layer and multi-layer (i.e., graphite-like) specimens.

3.1.3 Scanning Electron Microscopy and Graphene

As mentioned previously, optical microscopy is useful as a first step in materials characterization as it readily produces magnified two-dimensional images of a large variety of sample systems. On the other hand, the resolution achievable by optical microscopy is fundamentally limited by the wavelength of visible light. As such, in modern materials science studies, the scanning electron microscope (SEM) is typically employed to perform high-resolution (conventionally down to ~10 nm) structural characterization of sample surfaces. The increased spatial resolution achieved by SEM when compared to optical microscopy is based on the fact that it uses a high-energy (measured in kV) beam of electrons for imaging rather than visible light.

The basic operating principle of the SEM can be summarized as follows: An electron gun (e-gun) generates thermionically emitted electrons which are accelerated to high energies by a positively charged anode plate. The high-energy electrons passing through the anode are focused via electromagnetic lenses towards the sample surface to be investigated. Scanning coils are used to generate magnetic fields such that the electron beam is *scanned* over the sample surface in the lateral *x* and *y* directions. The electrons that reach the sample surface are called *primary electrons*. Primary electrons scatter from the sample surface and also promote the ejection of electrons from the atoms of the sample surface. Incident electrons bouncing from the sample surface with high energies as a consequence of elastic scattering are termed *backscattered electrons* which typically provide information about the chemical identity of the sample as their number depends on the atomic number of the species on the sample

surface. On the other hand, low-energy electrons that are emitted from the atoms of the sample surface due to inelastic scattering are called *secondary electrons* and are utilized to detect surface topography as their number depends on the angle formed by the incident electron beam and the structural features of the sample surface. Detectors dedicated to backscattered and secondary electrons coupled to a screen consequently convert the signals from incident electrons to optical images of the surface, sensitive to surface chemistry and topography, respectively (Figure 3.5) [52].
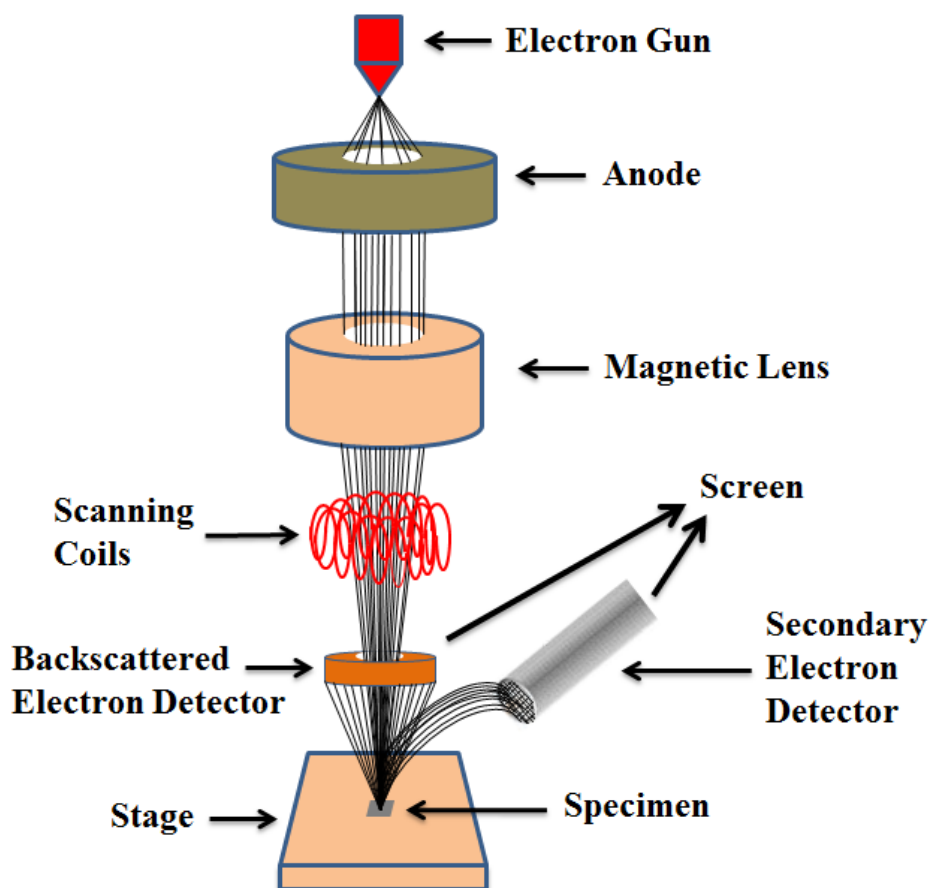
Figure 3.5 A simplified diagram of a scanning electron microscope (SEM).

Ernst Ruska (1906-1988) is the main person who is credited with the first design of an electron microscope, which eventually led to the awarding of the Nobel Prize in Physics in 1986. The very first version of a functional SEM was built by German Scientist Max Knoll in 1935 [53].

In the literature, SEM has been intensely used to investigate the structural and morphological features of graphene obtained via different means. In particular, SEM

has been employed to investigate CVD-grown graphene on copper foils, as well as CVD-grown graphene transferred onto SiO_2 /Si substrates, with the principle aim of observing micro-scale structural defects (such as wrinkles, tears, and folds), as well as the presence of contaminants and impurities [54-56].

3.1.4 Atomic Force Microscopy and Graphene

As already discussed in Chapter 1, one of the major inventions that has spearheaded the development of nanoscience and nanotechnology over the last few decades is the atomic force microscope (AFM). In its simplest form, AFM utilizes a very sharp, nanometer-scale *probe tip* attached to a micro-machined cantilever to scan a given sample surface with sub-nm lateral and vertical precision, in order to produce a three-dimensional map of the associated topography. The AFM is composed of four substantial elements which are (i) a micro-machined cantilever (typically made of Si, SiO_2 or Si_3N_4), (ii) a piezoelectric element typically called the *scan piezo*, (iii) a laser, and (iv) a four-quadrant photodetector. The sample is placed on the scan piezo, which is used to perform *raster-scanning* in the lateral *x*, *y* directions while the tip is under slight contact with the sample surface (normal loads typically on the order of a few nN). During scanning, the vertical deflection and the torsional twisting of the cantilever due to the normal and lateral forces experienced by the probe tip are detected via the laser beam reflected from the back side of the cantilever onto the four-quadrant photodetector. A feedback circuit is typically employed to keep the normal force (i.e., the deflection of the cantilever) at constant values during scanning by changing the vertical position of the sample via the scan piezo. A precise read-out of the vertical position of the scan piezo provides high-resolution (down to ~1 nm laterally and sub-nm vertically) topographical information about the sample surface (Figure 3.6). At the same time, detection of lateral forces via the torsional twisting of the cantilever allows conclusions to be made about the frictional properties of the sample surface with nm-scale spatial resolution.

As indicated earlier, Gerd Binnig and co-workers introduced the first AFM which operated in the above-described contact mode [8]. Afterwards, other operational modes of AFM (such as *tapping* and *noncontact* modes) were discovered [57]. Moreover, AFM is frequently utilized as an analysis tool for identifying the frictional,

electrical, and magnetic properties of a large number of sample surfaces [58]. A detailed description of the operating principle of AFM with respect to its use in nano-scale friction measurements [11] is provided in Chapter 4.
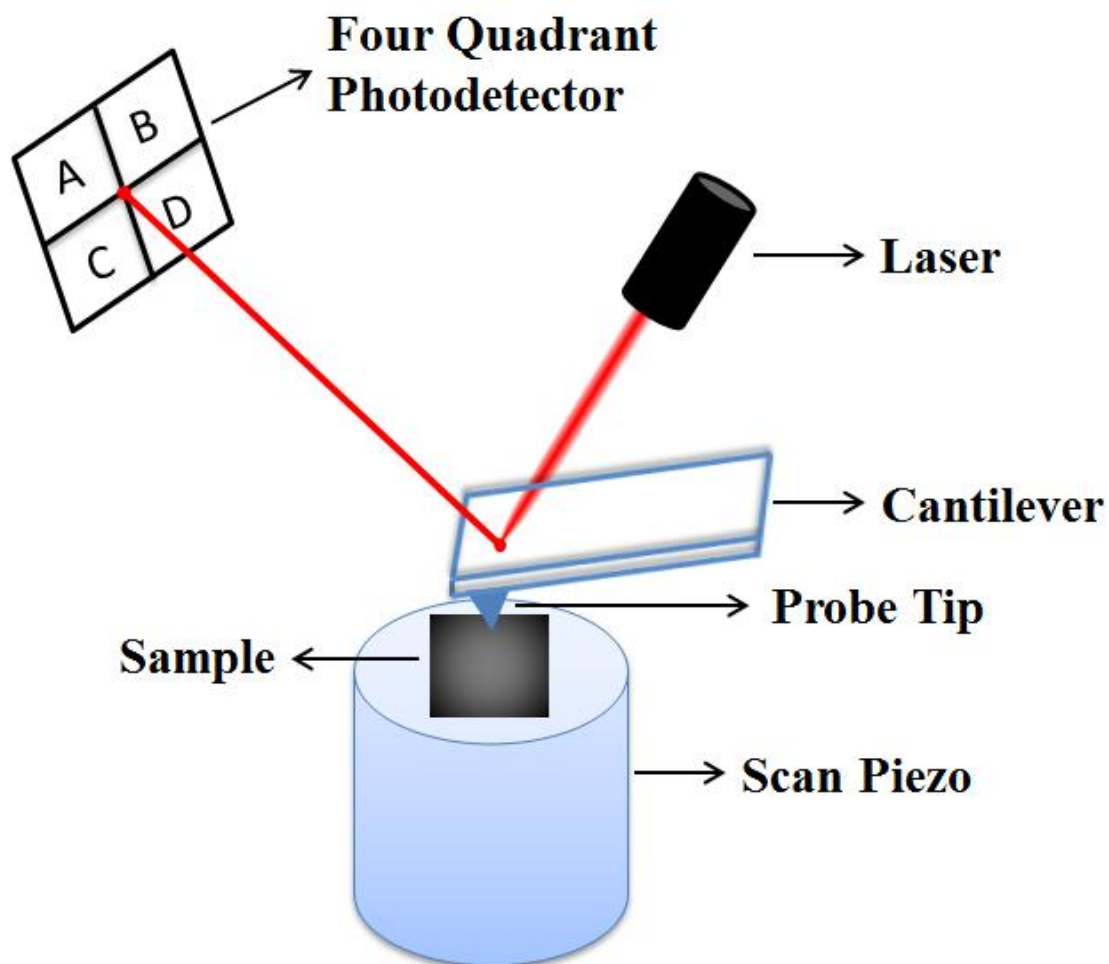
Figure 3.6 A basic illustration of an atomic force microscope (AFM) setup.

The main purpose of utilizing AFM in the structural and morphological characterization of graphene is two-fold: First, the thickness of graphene samples can be directly quantified by topographical imaging that allows a determination of number of layers. Additionally, the topography data obtained via AFM allow the user to image and study structural defects such as wrinkles, as well as torn and folded regions of the graphene samples, in addition to imaging contaminants from, e.g., transfer procedures. The topographical characterization of CVD-grown graphene is reported in several works in the literature. The height of single-layer graphene samples above the substrates onto which they have been transferred has been reported with great

variance, with results from 0.65 nm [59] all the way to 1.8 nm [46]. The reason behind the observed differences in graphene-substrate spacing (which is always significantly higher than the graphene-graphene spacing of ~0.33 nm) is attributed to the existence of adsorbed molecules between the graphene and the substrate, as well as the effect of wrinkles and folds in the transferred graphene sheets [46].

3.2 Structural Characterization of CVD-Grown Graphene on SiO$_2$/Si Substrates

Before a thorough structural and morphological characterization of CVD-grown graphene is performed, samples of sufficient quality need to be synthesized. As already mentioned in Chapter 2, the optimization of growth parameters such as temperature as well as flow rate and flow time of precursor and carrier gases is of prime importance to obtain high quality, predominantly single-layer graphene films on copper foils by the CVD method. As such, within the scope of this M.S. thesis, a large number of CVD experiments have been conducted with different combinations of growth parameters (Table 1). Subsequently, the corresponding graphene samples have been characterized via Raman spectroscopy and SEM such that the mean value of the I$_{2D/G}$ ratio (resulting from the measurement of ≥ 5 Raman spectra) and the uniformity of graphene coverage on SiO$_2$/Si substrates (in the sense that continuous graphene films without the dominant presence of defects such as tears and folds are obtained post-transfer) is evaluated. As a high I$_{2D/G}$ ratio and a high degree of uniformity are indicative of a reduced degree of microscopic defects, and consequently high quality, graphene samples obtained via growth conditions corresponding to the observation of high I$_{2D/G}$ ratios and a high degree of uniformity have been preferred in subsequent structural and nanotribological characterization experiments.

Table 3.1 The comparison of the quality of CVD-grown graphene samples obtained via different combinations of growth parameters

Exp. No.	Ar/H$_2$ gas flow rate (sccm)	Ar/H$_2$ gas flow period (process)	CH$_4$ gas flow rate (sccm)	CH$_4$ gas flow duration (min)	Temp. (°C)	Mean value of I$_{2D/G}$ in Raman Spectra	Uniformity of the graphene coverage
1	200	During annealing and growth	25	25	1000	2.69	**excellent**
2	200	During annealing	25	25	1000	2.57	**excellent**
3	700	During annealing and growth	25	25	1000	1.64	poor
4	700	During annealing	25	25	1000	1.8	poor
5	200	During annealing	50	25	1000	2.19	good
6	200	During annealing	75	25	1000	2.46	good
7	200	During annealing	150	25	1000	2.47	good
8	200	During annealing	250	25	1000	3.02	good
9	200	During annealing	25	5	1000	**3.31**	good
10	200	During annealing	25	10	1000	2.37	good
11	200	During annealing	25	15	1000	**3.24**	**excellent**
12	200	During annealing	25	20	1000	**3.25**	**excellent**
13	200	During annealing	25	45	1000	**3.16**	good
14	200	During annealing	25	20	1050	2.93	good
15	200	During annealing and growth	25	20	1000	**3.20**	**excellent**

As explained in Chapter 2, two different approaches involving the flow of Ar/H$_2$ during (a) annealing only or (b) during annealing *and* graphene growth (experiments 1, 3 and 15) can be employed in the CVD procedure. In order to evaluate the effect of simultaneous flow of the Ar/H$_2$ gas with CH$_4$ during graphene growth on structure and nanotribology, graphene samples featuring the highest I$_{2D/G}$ ratios and highest degrees

of uniformity in terms of coverage have been chosen from both groups (experiments 12 and 15) for further structural characterization. These samples are referred to as G-w/oH$_2$ and G-w/H$_2$, respectively, from now on.

Additionally, as already discussed, the post-transfer cleaning procedures that involve ultrasonic cleaning and annealing in Ar gas have been applied to as-transferred graphene samples of the G-w/oH$_2$ variety. These are referred to as G-UC and G-AGC, respectively. Consequently, four types of graphene films mentioned above (G-w/H$_2$, G-w/oH$_2$, G-UC and G-AGC) are investigated structurally and morphologically in the following sections of this chapter.

3.2.1 Structural Investigation of CVD-Grown Graphene via Optical Microscopy

Optical microscopy has been employed on CVD-grown graphene samples on copper foils and on SiO$_2$/Si substrates to investigate the coverage of graphene, as well as the potential occurrence of defects such as folds, tears, and ruptures. In optical microscopy images, areas of substrates covered by graphene appear darker than bare regions due to interference of visible light. It should be mentioned that an important advantage of optical microscopy is its non-destructive nature. For the work performed in this thesis, a commercial optical microscope has been utilized (Carl Zeiss Axio Imager.A2m, Figure 3.7).

A representative optical microscopy image of as-grown graphene on copper foil is presented in Figure 3.8, where the bare and graphene-covered regions of the copper foil can be readily discerned. The conformation of CVD-grown graphene on the topographical features of the bare copper foil should be noted.

In addition to as-grown graphene films on Cu foil, graphene films transferred onto SiO$_2$/Si substrates have also been investigated via optical microscopy. As CVD-grown films in our experiments tend to be continuous for relatively large distances (on the order of several mm and more), in order to distinguish transferred graphene samples from the substrate, optical images have been taken in the vicinity of the boundary of transferred films. Due to the limited spatial resolution of the optical microscopy method, representative data for the four types of graphene samples (G-w/H$_2$, G-w/oH$_2$,

G-UC and G-AGC) do not feature considerable differences in terms of the uniformity of surface coverage and the presence of contaminants (Figure 3.9). Clearly, experimental methods with higher spatial resolution (such as SEM and AFM) need to be employed to investigate the structure and morphology of CVD-grown graphene in more detail, as it is shown in Sections 3.2.3 and 3.2.4.

Figure 3.7 The optical microscope used for the work presented here (Carl Zeiss Axio Imager.A2m).
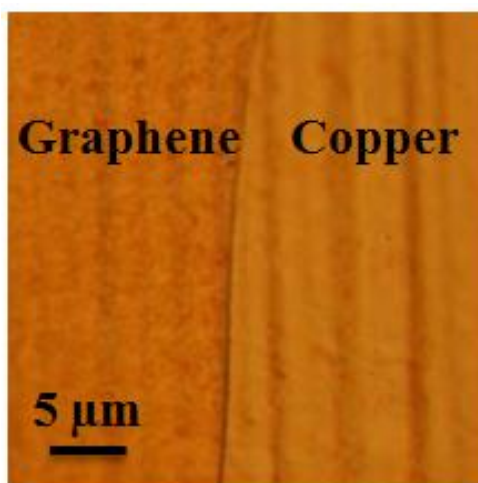
Figure 3.8 An optical microscopy image of CVD-grown graphene on copper.
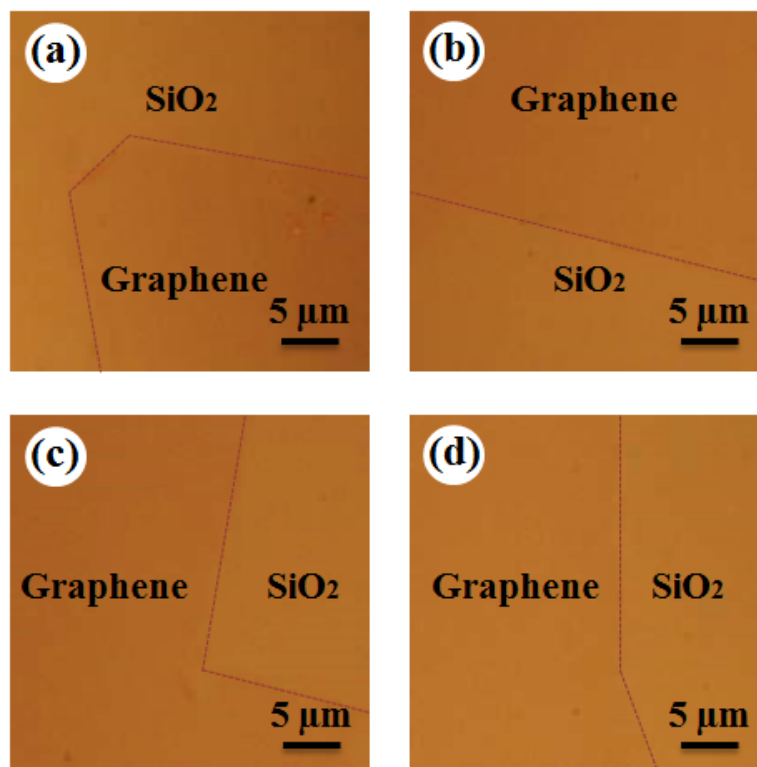
Figure 3.9 Optical microscopy images of CVD-grown graphene: (a) G-w/H$_2$, (b) G-w/oH$_2$, (c) G-UC, and (d) G-AGC.

3.2.2 Confirmation of Single-Layer Character of CVD-Grown Graphene via Raman Spectroscopy

As already discussed in Section 3.1.2, Raman spectroscopy provides useful information about the number of layers of graphene samples, as well as the associated density of microscopic defects. In particular a peak intensity ratio ($I_{2D/G}$) of ≥ 2 is indicative of single-layer character, and increasing peak intensity ratios are caused by decreasing density of defects (and consequently, higher quality graphene). In the literature, representative results for $I_{2D/G}$ ratios involving CVD-grown, single-layer graphene samples include 3.6 [46], 4.16 [59], and 5.55 [24].

To obtain the Raman spectra presented here, a combined SNOM/Confocal Raman Microscope has been employed (WITec Alpha300 S, Figure 3.10). Figures 3.11 and 3.12 include representative Raman spectra obtained at specific points on the four types of graphene samples investigated here (G-w/H$_2$, G-w/oH$_2$, G-UC and G-AGC). In order to demonstrate the relatively large variability in $I_{2D/G}$ ratios that one can obtain

during the measurements, spectra with relatively low values of $I_{2D/G}$ have been selected for Figure 3.11, while spectra with relatively high values of $I_{2D/G}$ are presented in Figure 3.12. Within this context, it should be emphasized that $I_{2D/G}$ values from several (at least 5) spectra obtained at different points of a given sample have been averaged to determine the overall quality of graphene samples, as shown in Table 1.
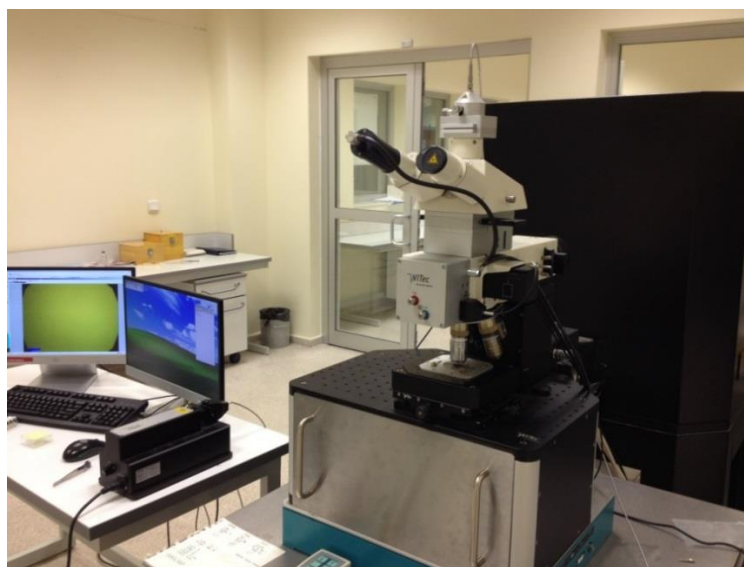
Figure 3.10 The combined SNOM/Confocal Raman Microscope (WITec Alpha300 S) used for the experiments presented in this thesis, available at the National Nanotechnology Research Center (UNAM).

An important point that is readily observable from Figures 3.11 and 3.12 is the fact that while post-transfer ultrasonic cleaning does not have an observable effect on $I_{2D/G}$ ratios, post-transfer annealing under Ar flow at 300 ^{o}C leads to a detectable increase in associated values. This finding is accompanied by an upshift in the position of the 2D peak, by 14 cm^{-1} (Figure 3.13). While the increase in the $I_{2D/G}$ ratios is at odds with certain results in the literature which point towards a decrease in the associated values after annealing under Ar [60, 61], the upshift in the 2D peak position is actually in-line with the literature, in the sense that an increase in the position of the 2D peak up to ~20 cm^{-1} upon annealing under Ar gas at temperatures up to 400 ^{o}C has been previously reported [60, 61]. While these results are interesting, it should be noted that further clarification of associated physical mechanisms is beyond the scope of this thesis.
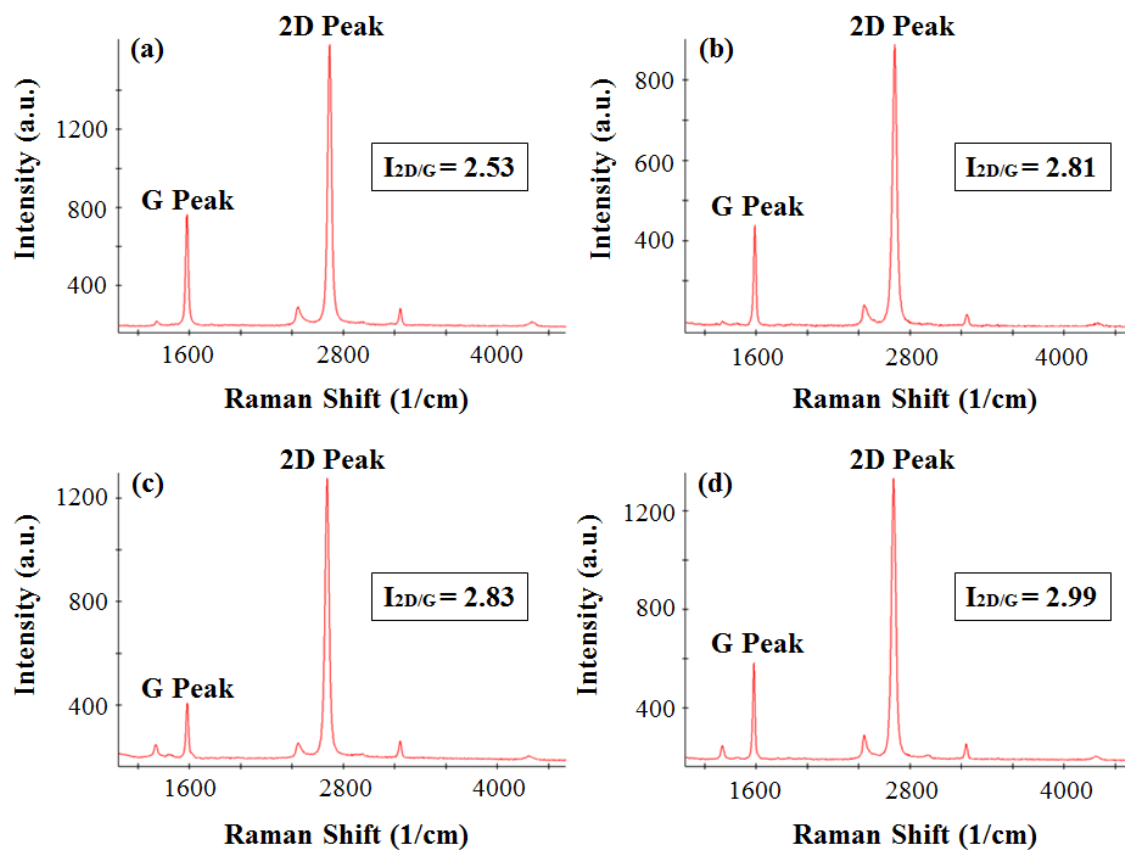
Figure 3.11 Selected Raman spectra of CVD-grown graphene samples: (a) G-w/H$_2$, (b) G-w/oH$_2$, (c) G-UC, and (d) G-AGC. Raman spectra featuring relatively low values of I$_{2D/G}$ are shown here.
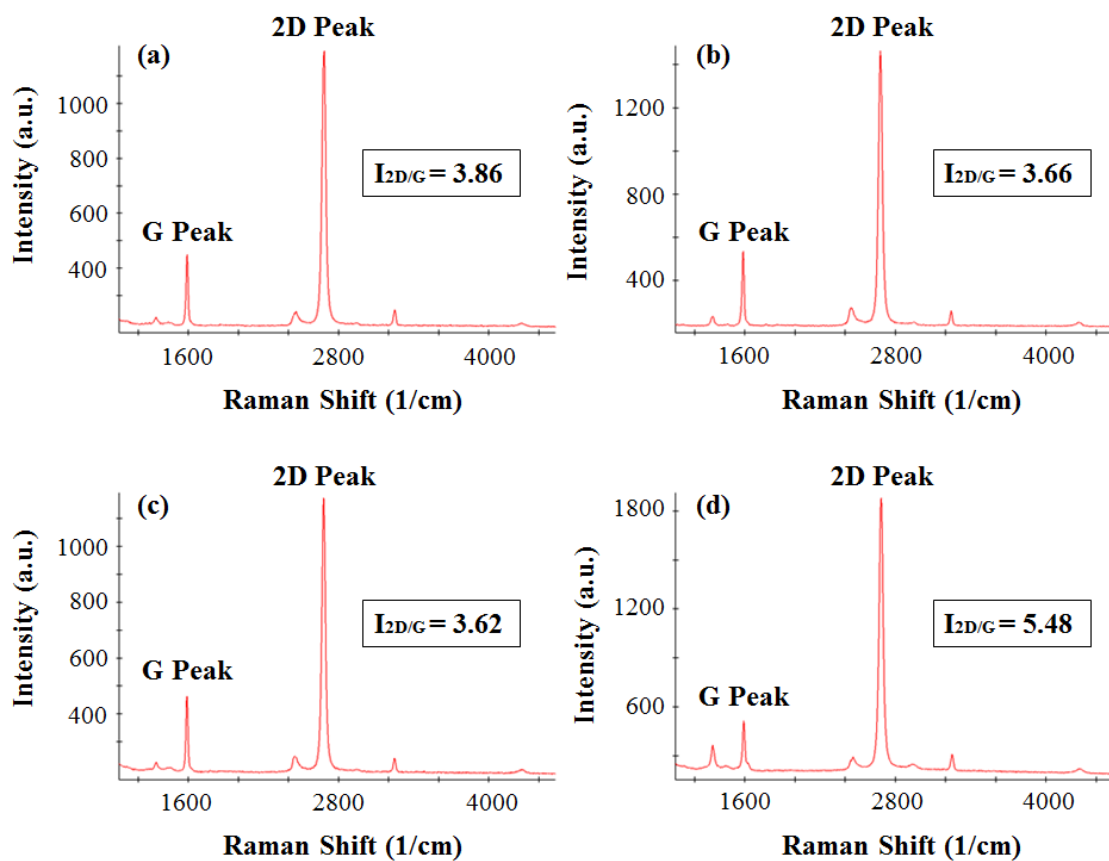
Figure 3.12 Selected Raman spectra of CVD-grown graphene samples: (a) G-w/H$_2$, (b) G-w/oH$_2$, (c) G-UC, and (d) G-AGC. Raman spectra featuring relatively high values of I$_{2D/G}$ are shown here.
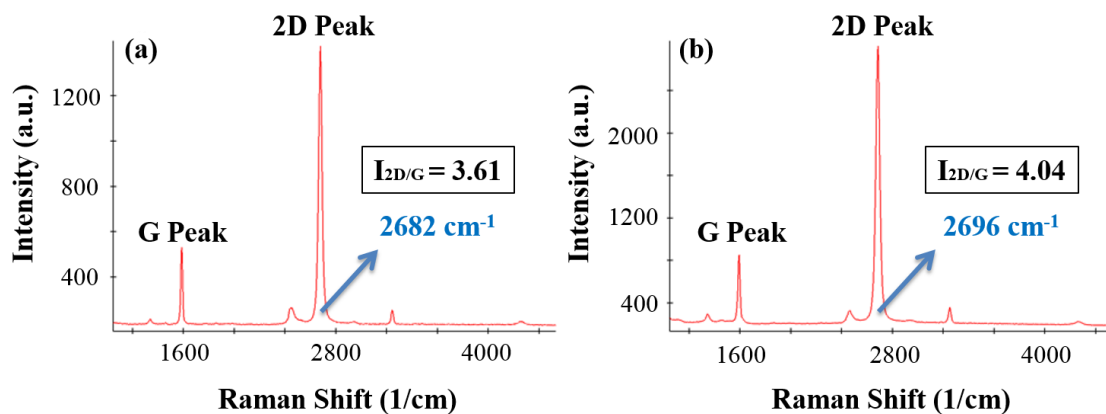
Figure 3.13 Representative Raman spectra of CVD-grown graphene (a) before post-transfer annealing, and (b) after annealing under Ar gas at 300 °C for two hours.

3.2.3 Structural and Morphological Investigation of CVD-Grown Graphene on SiO₂/Si Substrates via Scanning Electron Microscopy

As already pointed out, SEM has been used in this M.S. thesis to microscopically analyze the uniformity of the coverage of CVD-grown graphene on SiO_2/Si substrates and the associated structural defects. The main advantage of SEM when compared to the optical microscope is the fact that it features much higher spatial resolution. On the other hand, upon extended use, SEM may lead to sample contamination via deposition of amorphous carbon, originating either from residual hydrocarbons in the vacuum chamber and/or molecules present on the sample surface. As such, care needs to be exercised to limit the duration of SEM experiments.

The scanning electron microscope utilized for the characterization of the microstructural features of graphene (FEI Quanta 200 FEG) is depicted in Figure 3.14. Figure 3.15 shows the general appearance of CVD-grown graphene transferred onto SiO_2/Si substrates via a large-scale SEM image. As indicated earlier, certain defects such as tears and folds may occur on the graphene surface during the transfer process. Moreover, contaminants in the form of small *white* dots are sometimes detected on CVD-grown graphene samples. Representative SEM images featuring common structural defects and contaminants are provided in Figure 3.16. While the exact chemical nature and origin of the *white* dots are still under debate (see, e.g., the discussion in [62]), elemental analysis conducted via *energy dispersive X-ray spectroscopy* (EDX) in the SEM indicates that oxygen is involved, supporting the idea that the white dots are "most likely a product of oxidation upon exposure to ambient air and surface pretreatment by standardized hydrochloric acid procedures during copper foil manufacturing" [62]. Finally, representative SEM images of the four types of graphene samples investigated here (G-w/H₂, G-w/oH₂, G-UC and G-AGC) are provided in Figure 3.17, which do not show systematic differences in structure and morphology upon post-transfer cleaning.

Figure 3.14 The scanning electron microscope used for the experiments presented here (FEI Quanta 200 FEG), available at the National Nanotechnology Research Center (UNAM).
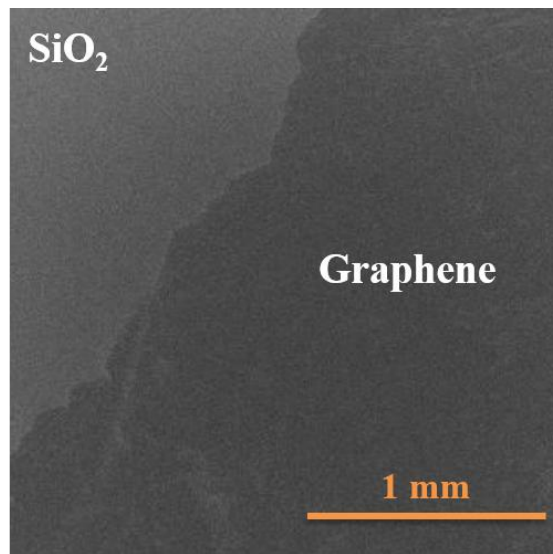
Figure 3.15 A large-scale SEM image which demonstrates overall graphene coverage on the SiO_2/Si substrate.
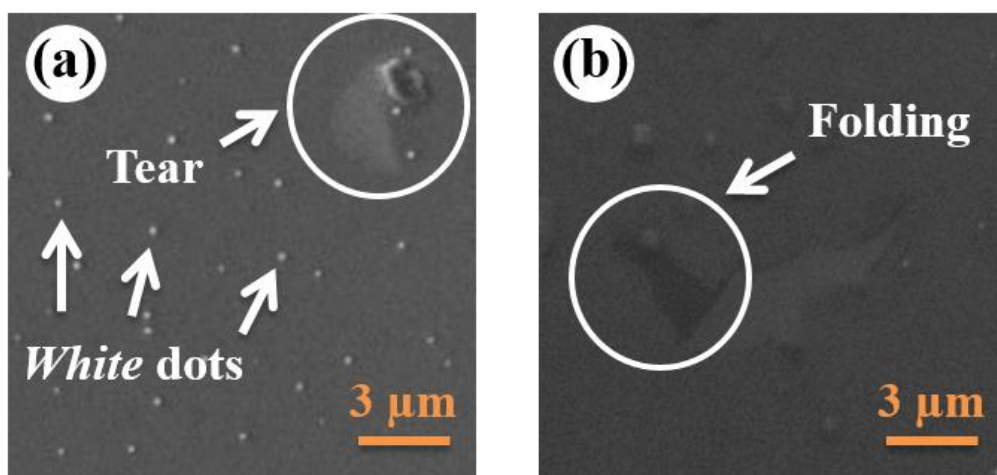
Figure 3.16 SEM images illustrating common structural defects and contaminants associated with CVD-grown graphene on SiO_2/Si substrates such as: (a) *White* dots and a torn area, (b) Folded area.
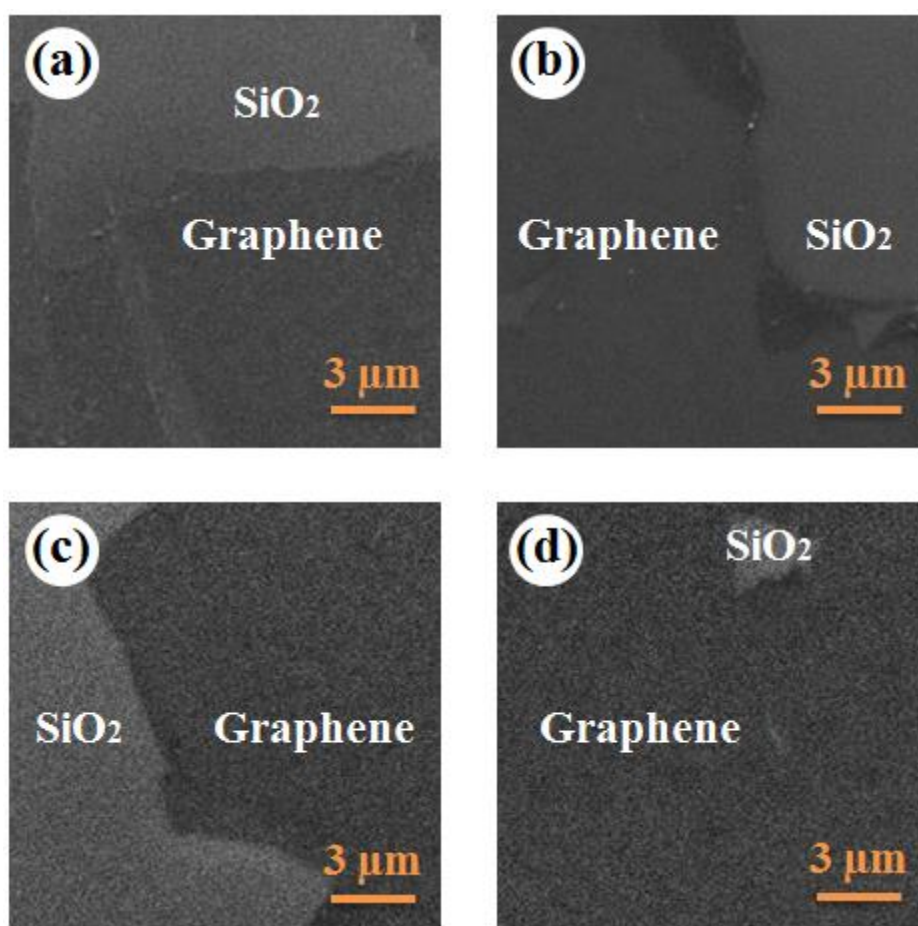
Figure 3.17 Representative SEM images of CVD-grown graphene: (a) G-w/H_2, (b) G-w/oH_2, (c) G-UC, and (d) G-AGC.

3.2.4 Structural and Morphological Investigation of CVD-Grown Graphene on SiO₂/Si Substrates via Atomic Force Microscopy

It has been discussed in Section 3.1.4 that atomic force microscopy (AFM) is particularly useful in (i) detecting the thickness of graphene samples on the substrates onto which they have been transferred and (ii) observing structural defects with high resolution. At this point, it should be mentioned that *wrinkles* are one of the most common structural defects associated with CVD-grown graphene (Figure 3.18) that are nevertheless not always straightforward to observe with optical microscopy or SEM [36]. Wrinkles arise during the cool-down step of the CVD process due to the substantial difference in the thermal expansion coefficients of graphene and copper foil, which subsequently leads to a build-up of in-plane stress on graphene. The stress is relieved by the formation of wrinkles, which are then readily observable in topographical AFM measurements of transferred samples, thanks to the very high spatial resolution of this method.
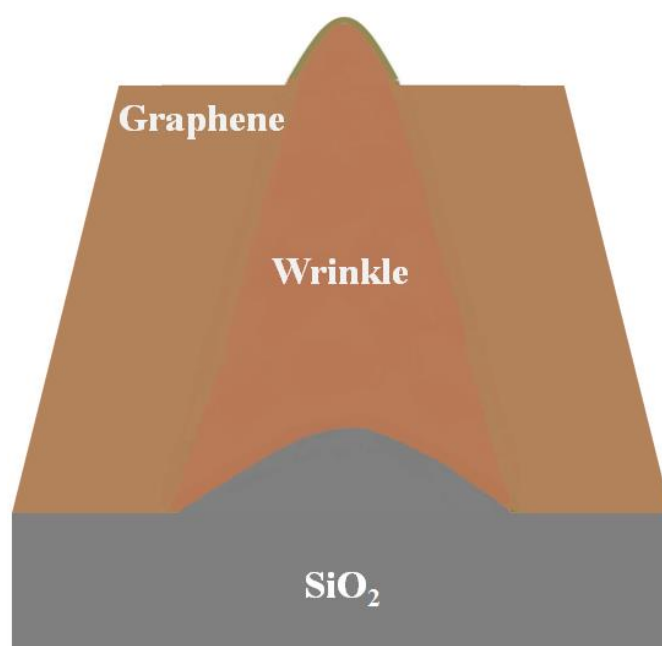
Figure 3.18 An illustration of a *wrinkle* on a graphene sample transferred onto a SiO₂/Si substrate.

The AFM studies presented in this thesis have been conducted with a commercial instrument (PSIA XE-100E, Figure 3.19) available at the National Nanotechnology Research Center (UNAM). A representative topographical AFM image of

CVD-grown graphene on SiO_2/Si is provided in Figure 3.20, together with its 3D representation, and height profiles over the graphene-SiO_2 boundary as well as over a typical wrinkle. Accordingly, the height of the transferred graphene with respect to the SiO_2 substrate is measured as ~1.45 nm, in line with certain values reported in the literature [46]. Moreover, the height of a representative wrinkle with respect to the graphene surface is given as ~2.8 nm. A statistical analysis of wrinkle heights conducted via AFM provides a mean value of 1.99 nm with a standard deviation of 0.869 nm.
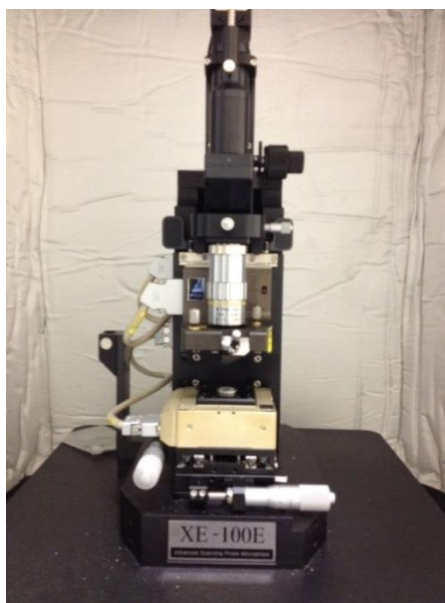
Figure 3.19 The atomic force microscope used for the experiments presented here (PSIA XE-100E), available at the National Nanotechnology Research Center (UNAM).

Finally, topographical AFM images of the four types of graphene samples investigated here (G-w/H_2, G-w/oH_2, G-UC and G-AGC) are provided in Figure 3.21, which illustrate in detail the existence of a considerable number of wrinkles on the samples, as well as the persistent existence of contaminants thought to be PMMA-residues, despite the post-transfer cleaning approaches employed - a finding that is supported by certain reports in the literature [44]. Please note that the high spatial resolution provided by the AFM method allows the investigation of graphene morphology and cleanliness in much higher detail when compared to optical microscopy and SEM.
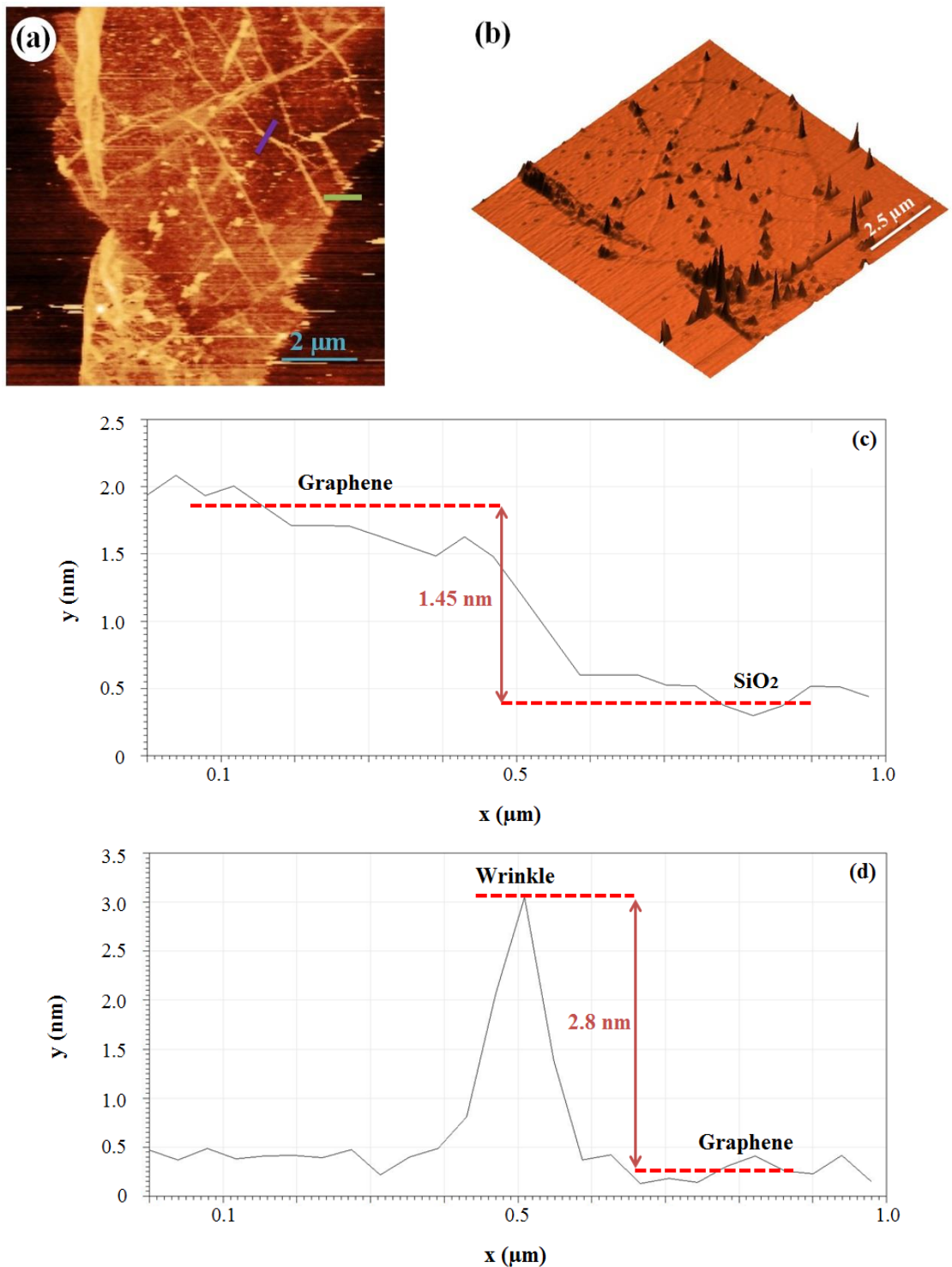
Figure 3.20 (a) A topographical AFM image of CVD-grown graphene on SiO_2/Si and (b) its 3D representation. (c) Representative height profile of the boundary between graphene and SiO_2/Si. (d) Representative height profile of a wrinkle on graphene. The height profiles in (c) and (d) have been recorded along the green and purple lines in (a), respectively.
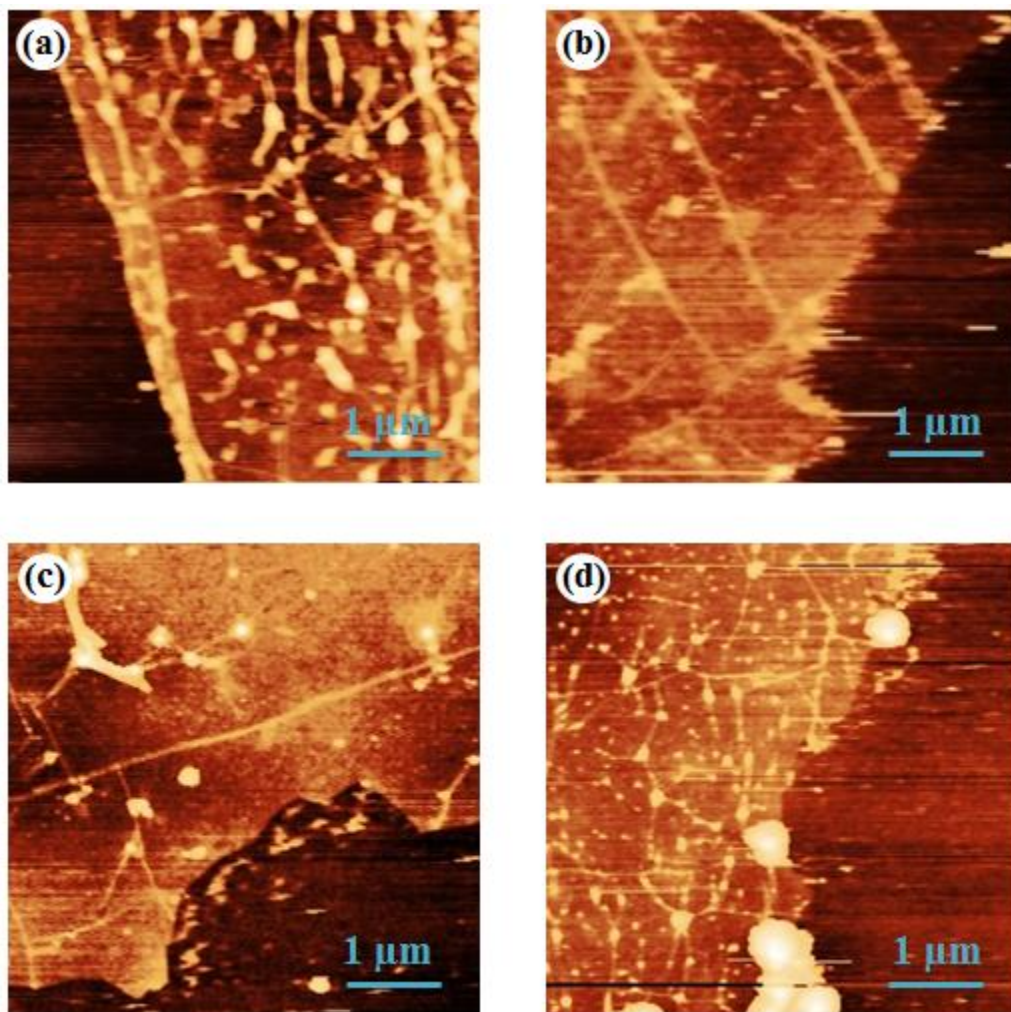
Figure 3.21 Topographical AFM images of CVD-grown graphene: (a) G-w/H$_2$, (b) G-w/oH$_2$, (c) G-UC, and (d) G-AGC.

Chapter 4

Nanotribological Characterization of CVD-Grown Graphene Transferred onto SiO$_2$/Si Substrates

4.1 Background

As already mentioned in previous parts of this M.S. thesis, atomic force microscopy (AFM), which is nowadays the most commonly utilized form of scanning probe microscopy (SPM), is useful not only in obtaining (sub-)nm resolution topographical maps of sample surfaces, but also in analyzing the associated mechanical, physical, and chemical properties [58]. Among the various physical quantities that may be precisely measured on sample surfaces by AFM, friction forces are of particular interest for the study presented here. The first demonstration that AFM may be used towards a precise characterization of frictional properties of sample surfaces was accomplished by Mate *et al*. in year 1987, when they introduced the friction force microscopy (FFM) mode that relies on recording the lateral forces experienced by the probe tip by recording the related torsional twisting of the cantilever [11]. Ever since its introduction, FFM has played a crucial role in nanotribology research as it has allowed researchers to investigate friction forces experienced at a structurally well-defined, *single asperity* contact (established by the sharp probe tip of the AFM

and the sample surface) in great detail as a function of experimental parameters, including but not limited to normal load, scanning speed, temperature and contact size [12, 63].

After the elegant demonstration that single-layer samples of graphene may be obtained by mechanical exfoliation of bulk graphite [14], a thorough characterization of mechanical, physical and chemical properties associated with this material have been performed in a series of publications [16]. In particular, based on its potential as an atomically-thick, solid lubricant suitable for use in nano- and micro-scale electro-mechanical systems where traditional fluid-based lubrication schemes fail due to increasing surface tension, the nanotribological properties of graphene have been the target of several published studies in the literature [19, 20, 64-68]. Specifically, in a pioneering work by C. Lee *et al*. a monotonous decrease in friction was measured for exfoliated graphene samples with increasing number of layers, such that single-layer graphene was found to exhibit the highest-friction values whereas bulk highly oriented pyrolytic graphite (HOPG) exhibited the lowest friction [19]. The findings have been explained by a so-called *puckering* effect that involves the enhanced build-up of graphene in front of the scanning probe tip at small number of layers (owing to reduced out-of-plane stiffness), which leads to enhanced friction [19].

On the other hand, for graphene samples grown epitaxially on SiC, friction was also measured via AFM, and it was found that bi-layer graphene demonstrated lower friction than both single-layer and bulk HOPG samples [20, 65]. These findings have been partially explained by an electron-phonon coupling mechanism [20, 65]. When it comes to a characterization of nanotribological properties of CVD-grown graphene, which is the main subject of this chapter in the thesis, there are very few studies: In particular, Egberts *et al.* have studied the nanotribological properties CVD-grown graphene *on copper foils* (i.e., pre-transfer), with the main discovery that friction forces on graphene patches on copper foils exhibit hysteretic behavior with changing normal load [66]. On the other hand, Fessler *et al.* have studied the effect of plasma-hydrogenation on nanotribological behavior of CVD-grown graphene on SiO_2/Si substrates [67]. Finally Kim *et al.* used a probe in the shape of a fused silica lens to investigate the friction and adhesion properties of CVD-grown graphene (on copper and nickel foils) transferred onto SiO_2/Si substrates [68].

Motivated by the studies mentioned above, this chapter includes a comprehensive nanotribological characterization of single-layer, CVD-grown graphene transferred onto SiO$_2$/Si substrates. In particular, and in contrast to literature, the effect of using different probe tips, growth conditions, and post-transfer cleaning procedures on the nanotribological properties is evaluated in detail; and results from several experiments involving different probe tips are averaged to deduce overall lubricative properties of graphene films on SiO$_2$/Si substrates. Additionally, the effect of *wrinkles* on measured friction forces is also investigated. Overall, the results presented in this chapter should contribute to an extensive evaluation of the potential of CVD-grown graphene as a solid lubricant suitable for practical applications.

4.2 Atomic Force Microscopy for Nanotribology Research

4.2.1 Operating Principle

Section 3.1.4 of this M.S. thesis provides an overview regarding the basic operating principle of AFM. Here, certain details about the use of AFM in nanotribology studies will be provided. The single asperity nature of the contact formed between the AFM probe and the sample under examination is a key aspect for precise nanotribological studies. The AFM probe is a sensitive and sharp tip, which is located at the end of the cantilever. In AFM, conventionally, the y-axis is taken to be parallel to the longitudinal dimension of the cantilever and the x-axis is taken to be parallel to the lateral dimension of the cantilever. The z-axis is located perpendicularly to the surface (Figure 4.1). As discussed earlier, during contact-mode scanning, the amounts of deflection and torsion undergone by the cantilever are detected via tracking the position of the laser beam that reflects from the backside of the cantilever and strikes a position-sensitive photodetector with four quadrants (A, B, C, D).
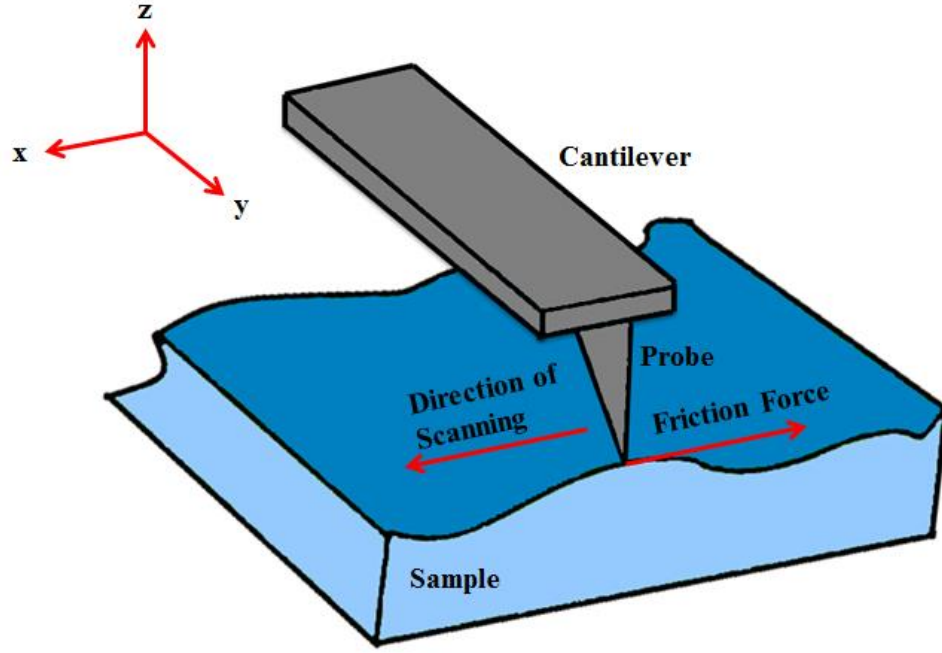
Figure 4.1 A basic sketch of atomic force microscopy, describing the friction force experienced by the AFM probe during scanning.

Within this context, it should be noted that the cantilever vertically deflects due to the normal interaction forces (F_n) acting between the probe and sample; and twists due to the lateral interaction forces (F_l). For the measurement of the normal load (force) between the probe and sample, the determination of the differential voltage signal intensity from the top (A and B) and bottom (C and D) quadrants of the photodetector is necessary. There is a linear relationship between the differential voltage signal intensity from the top and bottom parts of the photodetector ((A+B)-(C+D)) and the normal load (F_n), as seen below [69]:

$$F_n = (\theta_z \, ((A + B) - (C + D))) \tag{4.1}$$

where θ_z is the vertical force calibration factor.

Similarly, the voltage signal intensity difference between the left (A and C) and right (B and D) quadrants of the photodetector provides information about the lateral force (F_l). The lateral force is linearly proportional to the differential voltage signal intensity from left and right quadrants, as seen below [69]:

$$F_l = (\theta_x \, ((A + C) - (B + D))) \tag{4.2}$$

where θ_x is the lateral force calibration factor. During a typical AFM measurement, tracking the differential voltage signal intensity in Equation (4.2) while raster-scanning provides a map of lateral forces on the sample surface in terms of voltage units. The collected data are converted into force units by determining θ_x via calibration methods discussed in the literature and also mentioned below [70].
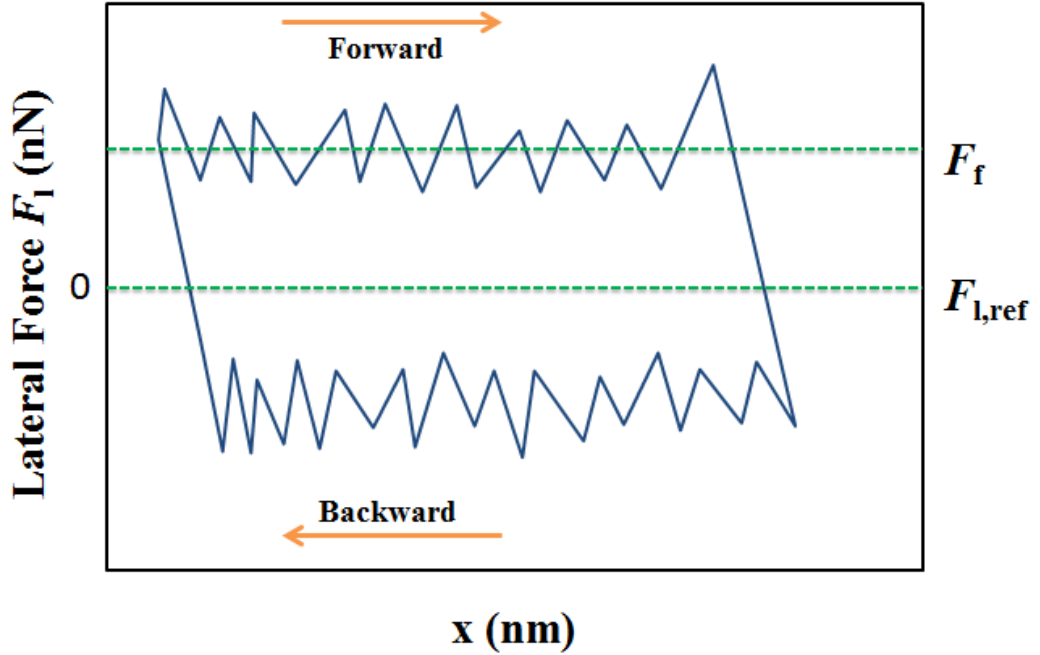
Figure 4.2 An illustration of a *friction loop* arising as a result of lateral forces with opposite signs recorded in the forward and backward scanning directions.

At the beginning of a typical AFM measurement, the laser spot is adjusted at the center of the four quadrant photodetector, so that the initial values for both F_n and F_l are taken as zero. However, during measurements, the reference position of the laser spot on the photodetector (corresponding to a reference lateral force value $F_{l,ref}$, which should be ideally zero) may shift either due to thermal effects or a coupling between the deflection and torsional twisting undergone by the cantilever. To prevent this issue from affecting quantitative lateral force measurements, friction force (F_f) values are always calculated by taking the *half-width* of *friction loops* formed by lateral forces recorded during forward and backward scanning of the same region (Figure 4.2) [71]. Please note the opposite signs of lateral forces recorded in the forward and backward scanning directions due to the opposite direction of torsional twisting undergone by the cantilever.

4.2.2 Force Calibration

The AFM provides scientists with precise information about the normal and lateral forces experienced by the probe while scanning over a particular surface, which is crucial for detailed nanotribological studies. To extract accurate force information, the normal spring constants of the cantilevers (k) as well as lateral force calibration factors (θ_x) must be determined.

The normal spring constants of rectangular cantilevers used in this work are determined via standard methods introduced in the literature [72]. In essence, the normal spring constant calibration method is related to the determination of the resonance frequency and mass of the cantilever. Thus, the normal spring constant of a typical rectangular cantilever used in our experiments is calculated by:

$$k = \rho_c \, h \, b \, L \, M_e \, w_{vac}^2 \tag{4.3}$$

where ρ_c is the density of the cantilever (for Si, 2.329 g/cm^3), h, b, and L are the thickness, width, and length of the cantilever (2 µm, 50 µm, 450 µm), respectively, M_e is the normalized effective mass which is taken as 0.2427 due to the fact that the aspect ratio of the cantilever (L/b) is higher than 5 [72], and w_{vac} is the angular resonance frequency of the cantilever in vacuum. As the magnitude of the resonance frequency of a typical rectangular cantilever drops by ~2% due to air damping under ambient conditions relevant for our experiments, this fact is taken into account during the determination of normal spring constants [72].

In addition to determining normal spring constant values, each AFM cantilever must be calibrated for lateral force measurements, by determining the corresponding θ_x values. As the intricate details of the standard lateral force calibration method are discussed in the literature [70], it should be sufficient to mention here that the calibration is performed via the recording of lateral forces on a standard reference sample with known structure (TGF11 silicon calibration grating, MikroMasch, Figure 4.3) as a function of increasing normal load, and by investigating the coupling between normal and lateral forces on the slopes of the underlying substrate.
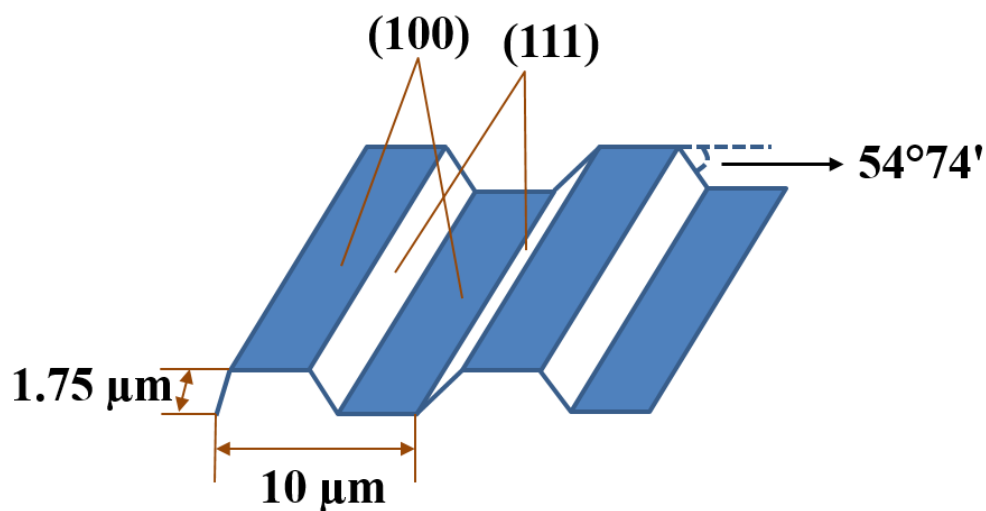
Figure 4.3 A schematic diagram of the surface structure of TGF11 silicon calibration grating used for the determination of lateral force calibration factors in this thesis.

To conclude this section, the normal spring constant and lateral force calibration factors of the five cantilevers (Nanosensors PPP-CONTR) used for the experiments reported in this chapter are provided in Table 4.1.

Table 4.1 The normal spring constants and lateral force calibration factors of the five cantilevers used for the nanotribology work presented in this thesis

Cantilever Number	Normal Spring Constant (N/m)	Lateral Force Calibration Factor (nN/V)
1	0.24	10
2	0.16	15
3	0.24	12
4	0.15	19
5	0.13	30

4.3 Nanotribological Characterization of CVD-Grown Graphene on SiO₂/Si Substrates via AFM

Within the scope of this M.S. thesis, nanotribological characterization of single-layer graphene films grown via CVD on copper foils and transferred onto SiO$_2$/Si substrates (as detailed in Chapter 2) has been carried out using contact mode AFM (in its FFM mode) under ambient conditions. In particular, emphasis has been placed on evaluating the effect of using different probes, as well as employing different growth conditions, and applying different post-transfer cleaning procedures on the frictional behavior of graphene samples. Lateral force maps have been recorded on regions in the vicinity of the boundaries of transferred graphene on SiO$_2$/Si substrates, as a function of increasing normal load (F_n), in order to be able to compare and contrast the frictional properties of both materials. Additionally, it has been decided to evaluate the effect of *wrinkles* of CVD-grown graphene samples on frictional behavior, based on the observation that these structural defects are frequently encountered during the experiments (as demonstrated in Chapter 3).

4.3.1 Dependence of Friction Forces Measured on CVD-Grown Graphene, Wrinkles, and the SiO₂/Si Substrate on Normal Load

Ever since the introduction of the FFM method [11], the relationship between the observed friction force (F_f) and the normal load (F_n) values on various materials has been investigated in detail in a number of studies [12]. In particular, for some material systems, it was found that the friction force (F_f) linearly increases with increasing normal load (F_n) [73], while in other studies the relationship between the friction force (F_f) and the normal load (F_n) could be described by a Hertzian contact mechanics approach ($F_f \sim F_n^{2/3}$) [74, 75]. On the other hand, the dependence of friction forces on normal load for graphene samples has been rarely investigated, with no conclusive determination of the functional form of the dependence of F_f on F_n (see, e.g., [64, 66]).

Along this line of research, friction forces recorded on CVD-grown graphene, increased friction forces encountered at wrinkles, as well as friction forces on the SiO_2/Si substrate have been investigated as a function of normal load in this thesis.
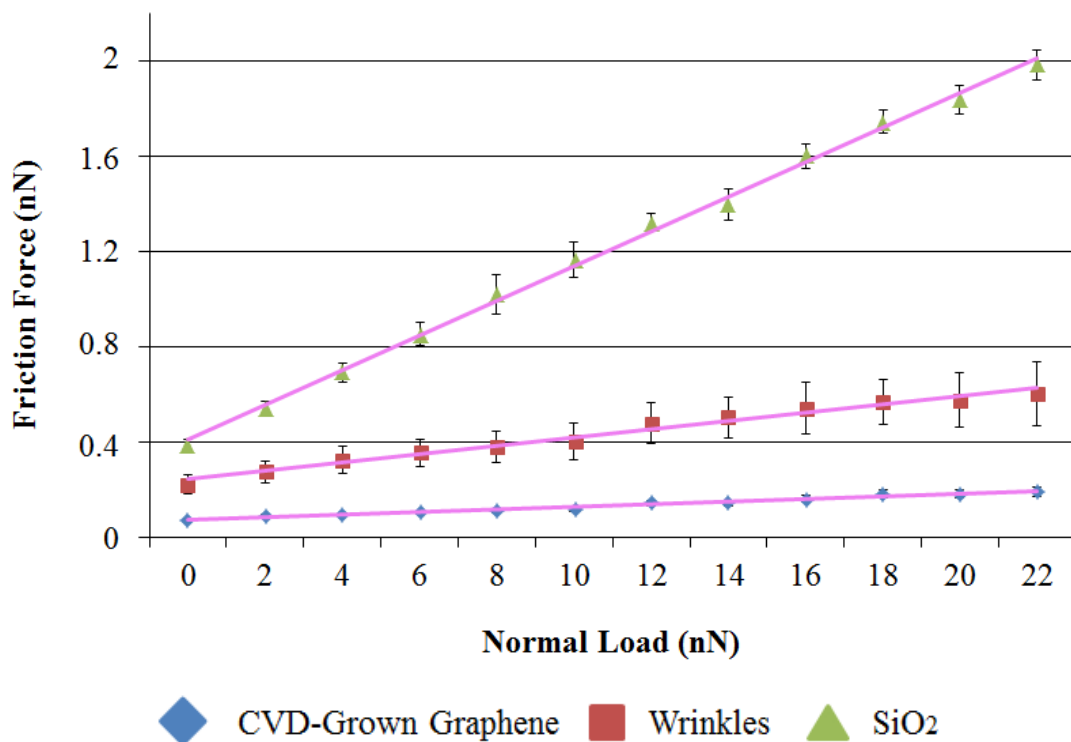
Figure 4.4 Representative measurements of the dependence of friction force (F_f) on normal load (F_n) for CVD-grown graphene, wrinkles, and the SiO_2/Si substrate, together with linear fits to the data. The error bars for measurements on CVD-grown graphene and SiO_2/Si substrate have been determined by considering the standard deviation in friction forces measured on multiple regions of a given lateral force map, while the error bars for the measurements on wrinkles have been determined by considering friction forces measured on 10 individual wrinkles.

Results of a representative measurement acquired with a single AFM probe are provided in Figure 4.4. As one can easily infer from the data, the SiO_2/Si substrate exhibits the highest absolute F_f values, followed by wrinkles and CVD-grown graphene. Thus, the *lubrication* properties of CVD-grown graphene on the SiO_2/Si substrate become apparent, as a significant reduction in absolute F_f values. Additionally, it is observed that the data can be fit reasonably well in a linear fashion. To eliminate the effect of potentially different degrees of adhesion exhibited by the

SiO$_2$/Si substrate when compared to CVD-grown graphene on measured absolute F_f values, tribological properties may be straightforwardly quantified by the slopes of linear fits applied to the data, to determine *coefficients of friction* (μ). While the data presented in Figure 4.4 already demonstrates that not only absolute F_f values, but also μ values are significantly lower on CVD-grown graphene when compared to SiO$_2$/Si ($\mu_{Graphene}$: 0.005, $\mu_{Wrinkle}$: 0.02, μ_{SiO2}: 0.07); a related, comprehensive analysis of lubrication properties of CVD-grown graphene is presented in Section 4.3.3.

Finally, the increase in F_f values measured on wrinkles is attributed to the sudden change in topography induced by them, in accordance with the so-called ratchet effect [76]. Thus, the existence of wrinkles on CVD-grown graphene samples should be taken into account when evaluating their potential use as solid lubricants.

4.3.1.1 Effect of Different Growth Conditions on Friction

As stated in Chapters 2 and 3, two sets of graphene samples with different growth conditions have been considered in our experiments (experiments numbered 12 and 15 in Chapter 3, referred to as G-w/oH$_2$ and G-w/H$_2$, respectively), differing in whether Ar/H$_2$ flow has been restricted to the annealing stage only or whether it has been applied during graphene growth, as well. The nanotribological properties of the two graphene samples are compared in Figure 4.5, with the same probe. It is evident from the comparison that the absolute values of friction force are comparable to a great extent between the two CVD-grown graphene samples, with the G-w/oH$_2$ variety exhibiting slightly smaller forces. It should be noted that the slight difference in F_f values observed on the substrates can be attributed to differences in mean nanometer-scale roughness.

On the other hand, when the lateral force maps associated with the two varieties of samples are investigated (Figure 4.6), it is observed that the G-w/oH$_2$ variety generally exhibits a lower density of wrinkles and structural defects when compared to the G-w/H$_2$ variety. As such, graphene samples of the G-w/oH$_2$ variety have been employed for the results presented in the following sections of this chapter.
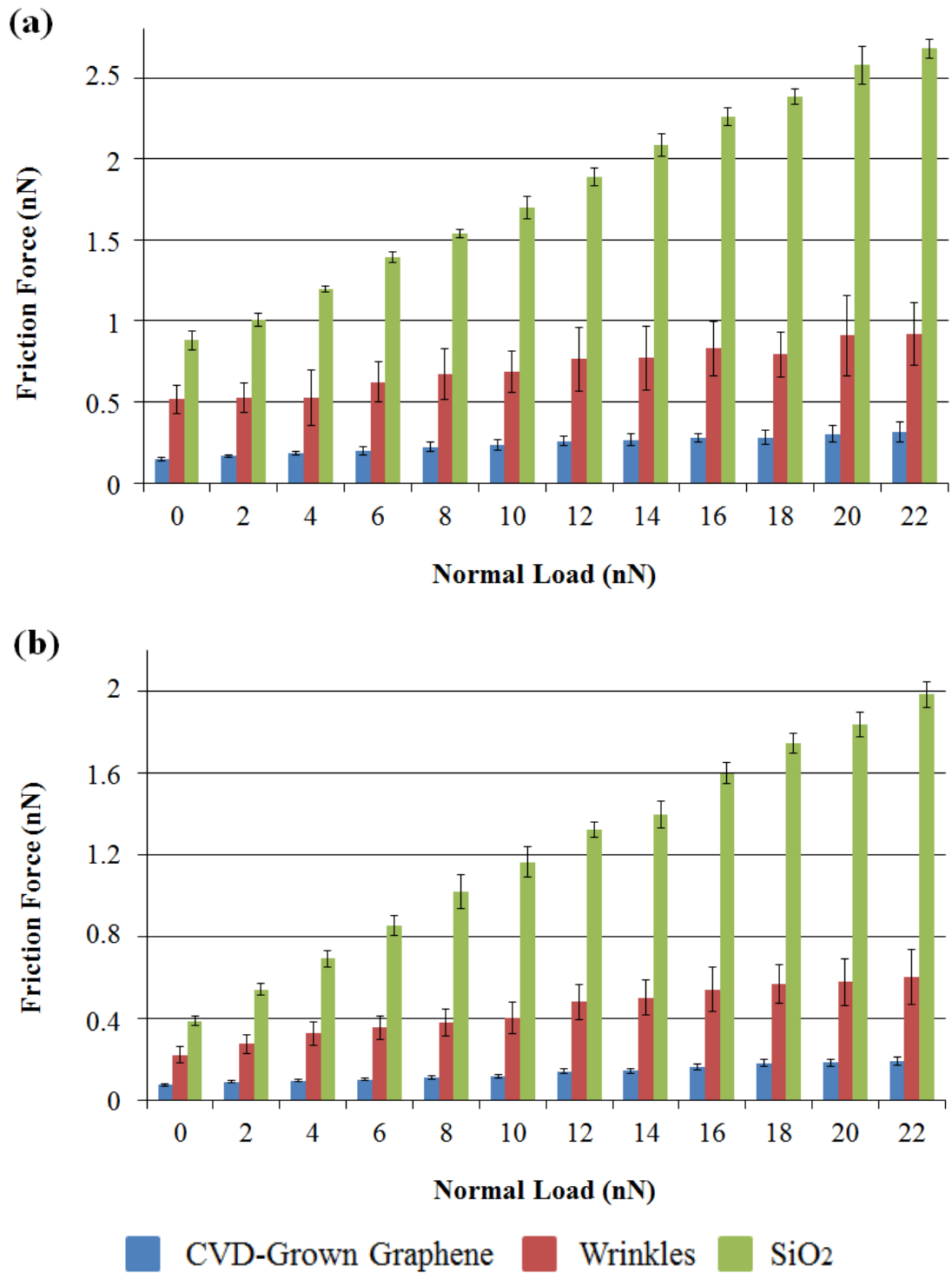
Figure 4.5 Graph detailing the dependence of friction force (F_f) on normal load (F_n) for CVD-grown graphene, wrinkles, and the SiO_2/Si substrate, for samples of the (a) G-w/H_2 and (b) G-w/oH_2 variety.
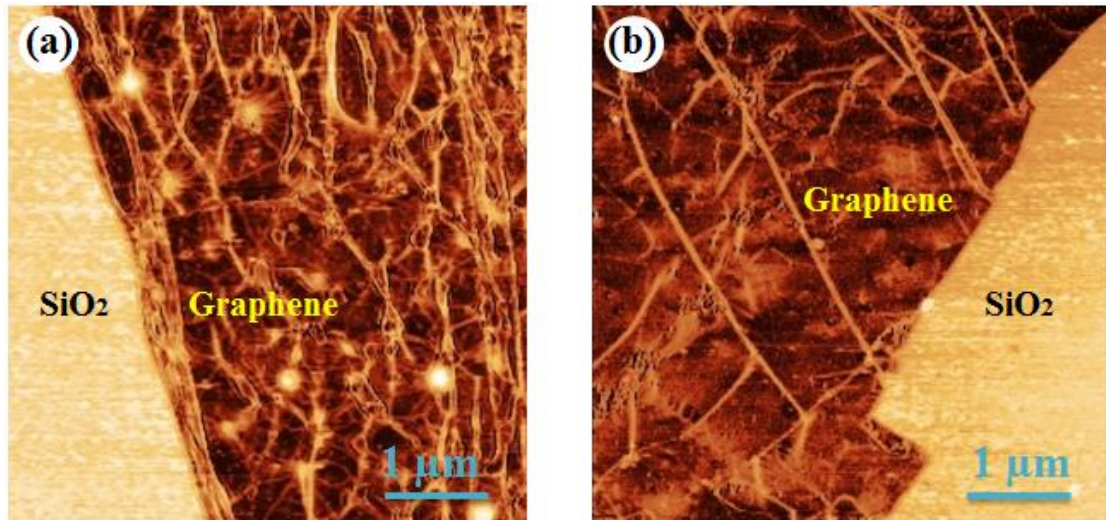
Figure 4.6 Lateral force maps of CVD-grown graphene on SiO_2/Si substrates for samples with two different growth conditions: (a) G-w/H_2 and (b) G-w/oH_2. Dark regions correspond to lower friction forces.

4.3.1.2 Effect of Using Different Probes (Tips) on Friction

It is well-known in the nanotribology community that the specific nanometer-scale structure and chemistry of the AFM probes (i.e., tips) may affect measured friction force values significantly [12]. Therefore, as indicated in Section 4.2, several different tips have been employed to perform the friction force measurements presented here. The results of F_f vs. F_n experiments performed on CVD-grown graphene, wrinkles, and SiO_2/Si substrates, conducted with three different probes, is presented in Figure 4.7. As expected, the SiO_2/Si substrate exhibits the highest absolute F_f values, followed by wrinkles and CVD-grown graphene, for all three tips. On the other hand, it is observed that a significant degree of variability is observed in measured F_f values from one tip to another, with Tip 2 generally exhibiting the highest friction. To eliminate the effect of using different tips on a rational evaluation of the lubrication properties of CVD-grown graphene, the *ratios* of *coefficients of friction* μ (as determined by linear fits to F_f vs. F_n data) measured for CVD-grown graphene and SiO_2/Si substrates ($\mu_{Graphene}/\mu_{SiO2}$) have been determined for each tip and consequently averaged to obtain general *lubrication ratios* in Section 4.3.3.
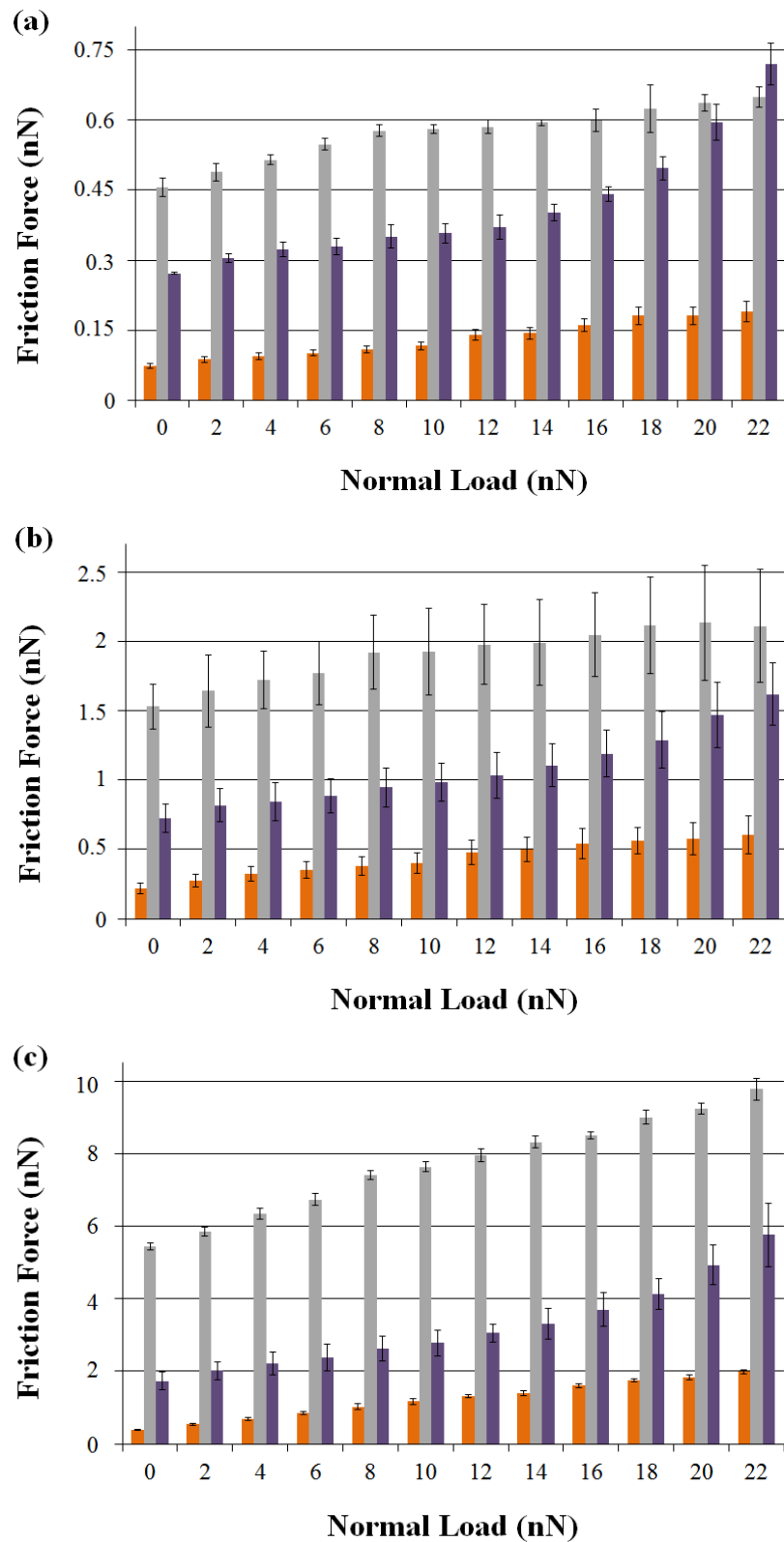
Figure 4.7 Graph detailing the dependence of friction force (F_f) on normal load (F_n) for (a) CVD-grown graphene, (b) wrinkles, and (c) the SiO$_2$/Si substrate, for three different tips (Tip 1: orange, Tip 2: grey, Tip 3: purple).

It should be noted that certain degradations associated with tip apexes occur during the measurements, sometimes resulting in appreciable enlargement of the apex radius and/or contaminations by, e.g., post-transfer chemical residues on the sample surface. For instance, the significant increase in F_f observed for Tip 3 in Figure 4.7(a) after 18 nN is tentatively attributed to such a structural/chemical change. In order to evaluate whether significant degradation of tip apexes has occurred during the AFM measurements, SEM images of selected tip apexes have been acquired before and after each experiment. A comparison describing a particularly severe degradation of a certain tip apex (Tip 3) is depicted in Figure 4.8. While such degradations of sliders are expected to also occur during potential practical implementations of CVD-grown graphene as a solid lubricant, it should be mentioned that the approach involving the calculation of $\mu_{Graphene}/\mu_{SiO2}$ ratios discussed above still allows a meaningful evaluation of lubrication performance under such conditions.
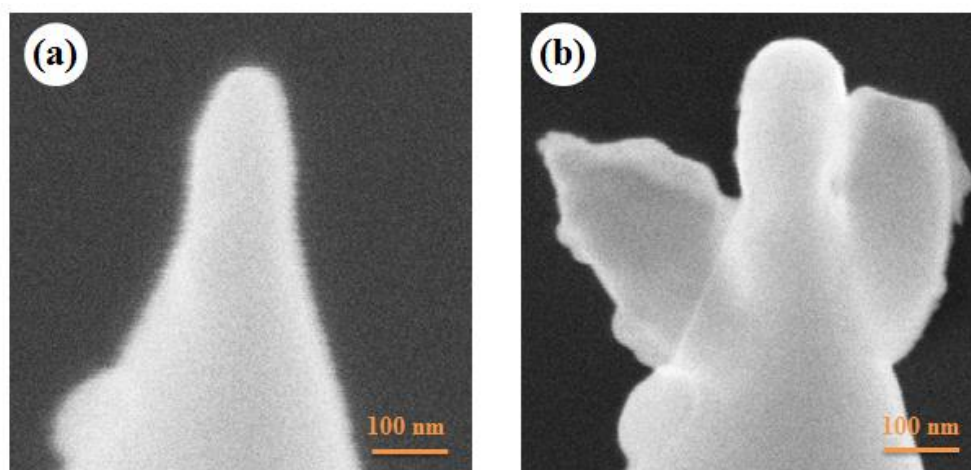
Figure 4.8 SEM images of the apex of Tip 3: (a) before, and (b) after AFM measurements, showing severe degradation.

4.3.1.3 Effect of Different Post-Transfer Cleaning Procedures on Friction

As indicated in Chapter 2, two post-transfer cleaning procedures have been optionally applied on CVD-grown graphene samples transferred onto SiO_2/Si substrates: (i) ultrasonic cleaning in acetone and isopropanol (G-UC) and (ii) Ar-gas annealing at 300 ^{o}C for two hours (G-AGC). Subsequently, the effect of post-transfer cleaning on the tribological behavior of CVD-grown graphene and wrinkles has been investigated (Figures 4.9 and 4.10).
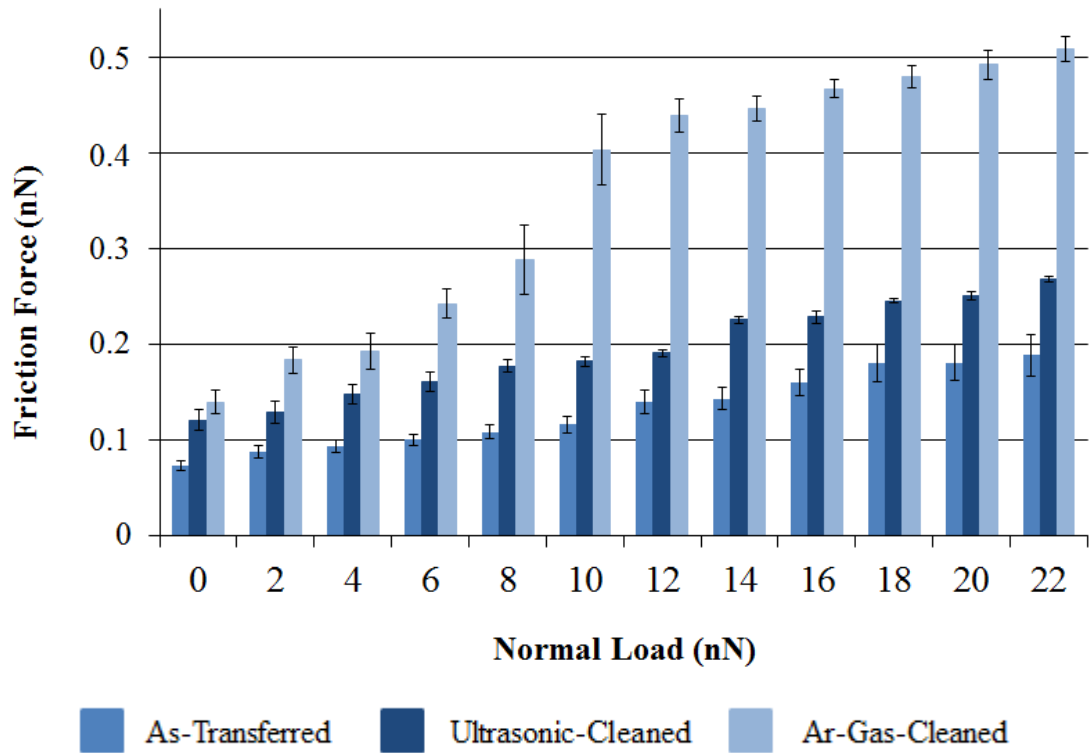
Figure 4.9 Graph detailing the dependence of friction force (F_f) on normal load (F_n) for as-transferred and post-transfer-cleaned CVD-grown graphene samples. Data acquired with Tip 1.

Figure 4.9 presents a comparison of tribological behavior of as-transferred and post-transfer-cleaned graphene samples in terms of F_f vs. F_n behavior, obtained with Tip 1. It is observed that the Ar-gas-cleaned sample exhibits the highest absolute friction force values, followed by the ultrasonic-cleaned sample, with the as-transferred graphene sample exhibiting the lowest friction forces. The same trend is observed for wrinkles (Figure 4.10). It should be indicated that, from this comparison alone, it is not possible to determine the origin of the increase in absolute friction values as the cleaning procedure itself, and not structural/chemical changes in the apex that occur during the experiments. As such, in order to reliably compare the lubrication performance of as-transferred and post-transfer-cleaned graphene samples on SiO_2/Si substrates, the previously mentioned approach involving the calculation of $\mu_{Graphene}/\mu_{SiO2}$ ratios has been employed in Section 4.3.3, with results being averaged for all tips used in this experimental study.

59
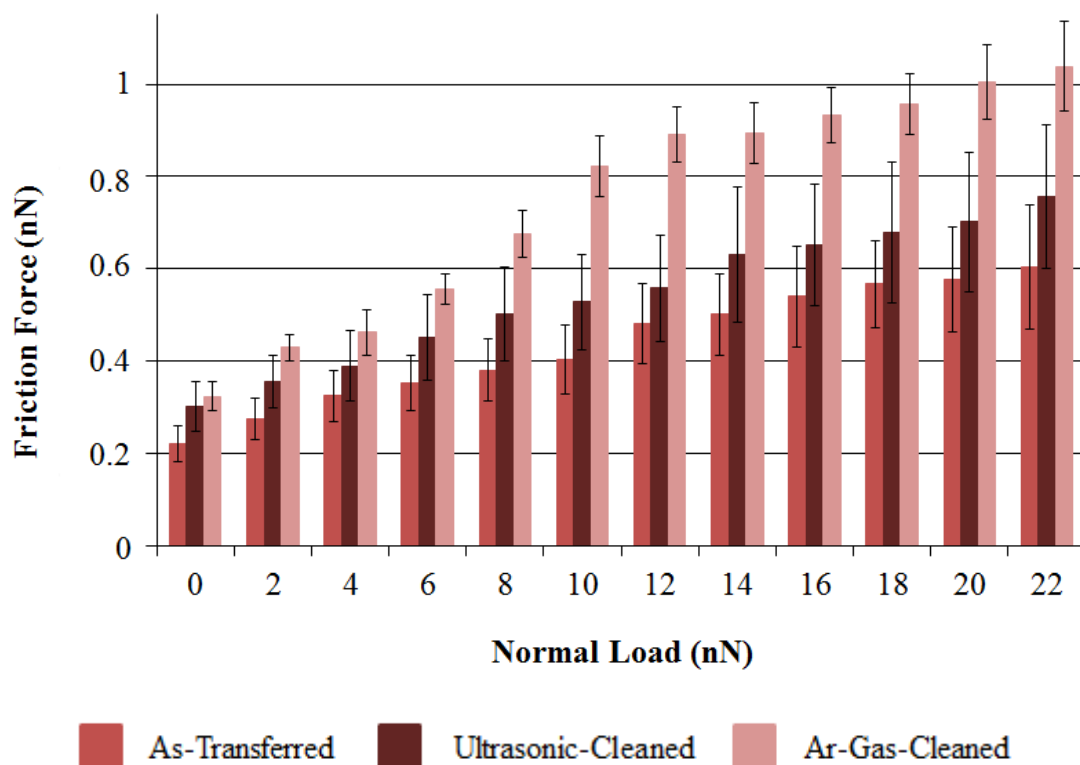
Figure 4.10 Graph detailing the dependence of friction force (F_f) on normal load (F_n) for wrinkles on as-transferred and post-transfer-cleaned CVD-grown graphene samples. Data acquired with Tip 1.

On the other hand, assuming structural/chemical changes in the tip apex are not the dominant factor leading to increased friction in ultrasonic-cleaned samples, microscopic structural damage on the graphene itself due to the cavitation bubbles arising during ultrasonic cleaning may be the physical reason for increased friction. Having said that, the physical mechanism leading to increased friction in Ar-gas-cleaned samples is currently unclear, with a hypothesis presented in Section 4.3.3. Finally, representative lateral force maps acquired on post-transfer-cleaned samples are presented in Figure 4.11, showing that a significant removal of chemical residues has not been achieved with either method (as indicated earlier).
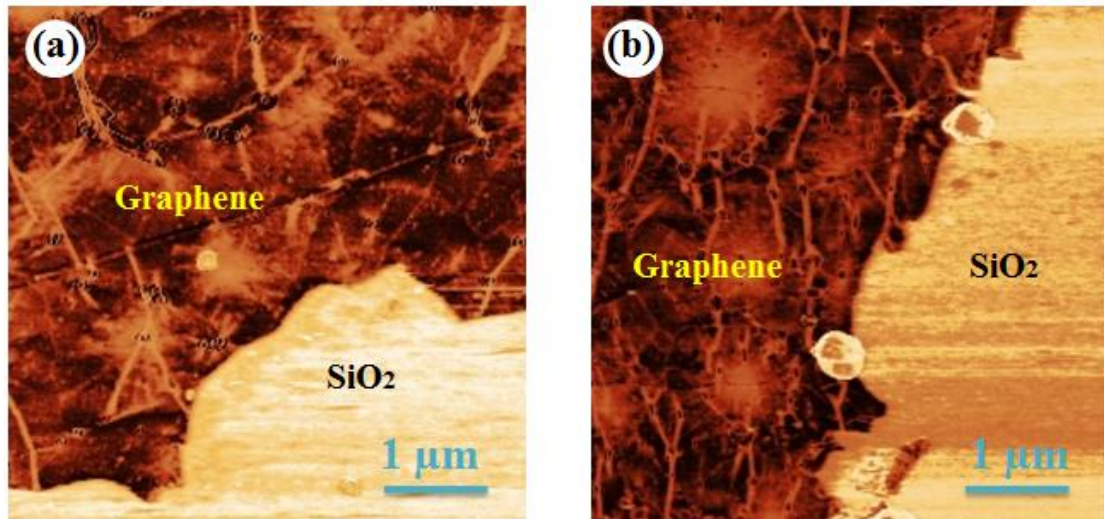
Figure 4.11 Lateral force maps of (a) ultrasonic-cleaned (G-UC), and (b) Ar-gas-annealed (G-AGC) samples. Dark regions correspond to lower friction forces. Data acquired with Tip 1.

4.3.2   Comparison with Lateral Force Measurements of Exfoliated Graphene

As already mentioned multiple times, apart from the CVD method, there are alternative methods for preparing graphene. Among these, the most common one involves the mechanical exfoliation of bulk HOPG [14, 15], which typically produces single-layer graphene flakes of much smaller size (tens of μm laterally) when compared to CVD. While too small for most practical applications, the nanotribological properties of mechanically-exfoliated graphene have been nevertheless the subject of certain fundamental studies [19, 64]. As part of this M.S. thesis, we have performed AFM experiments to compare the lubrication performance of CVD-grown graphene samples to mechanically-exfoliated ones.

Figure 4.12 presents representative lateral force maps of CVD-grown and mechanically-exfoliated graphene samples on SiO_2/Si substrates. Of particular note is the absence of wrinkles on the mechanically-exfoliated sample. The frictional properties of the two varieties of graphene are compared in Figure 4.13, which also provides the corresponding tribological data for the respective SiO_2/Si substrates (all acquired with Tip 3). While absolute friction force values look very similar for the two graphene samples until a normal load of 18 nN (at which point the tip might have undergone a structural/chemical change, as discussed earlier), a thorough comparison

61

of lubrication performance involving $\mu_{Graphene}/\mu_{SiO2}$ ratios and multiple tips is provided in Section 4.3.3. Finally, Figure 4.14 presents, for mechanically-exfoliated graphene, the results of F_f vs. F_n experiments for two different tips, highlighting again the role that the tip apex plays in nanotribological studies.
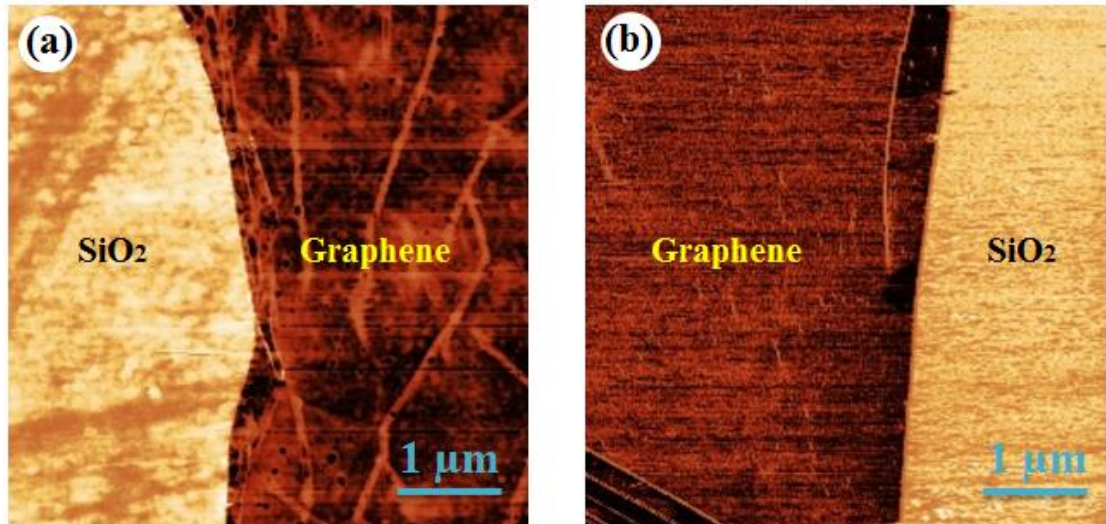
Figure 4.12 Lateral force maps of (a) CVD-grown and (b) mechanically-exfoliated single-layer graphene samples on SiO_2/Si substrate. Dark regions correspond to lower friction forces. Data acquired with Tip 3.

(a)

(b)
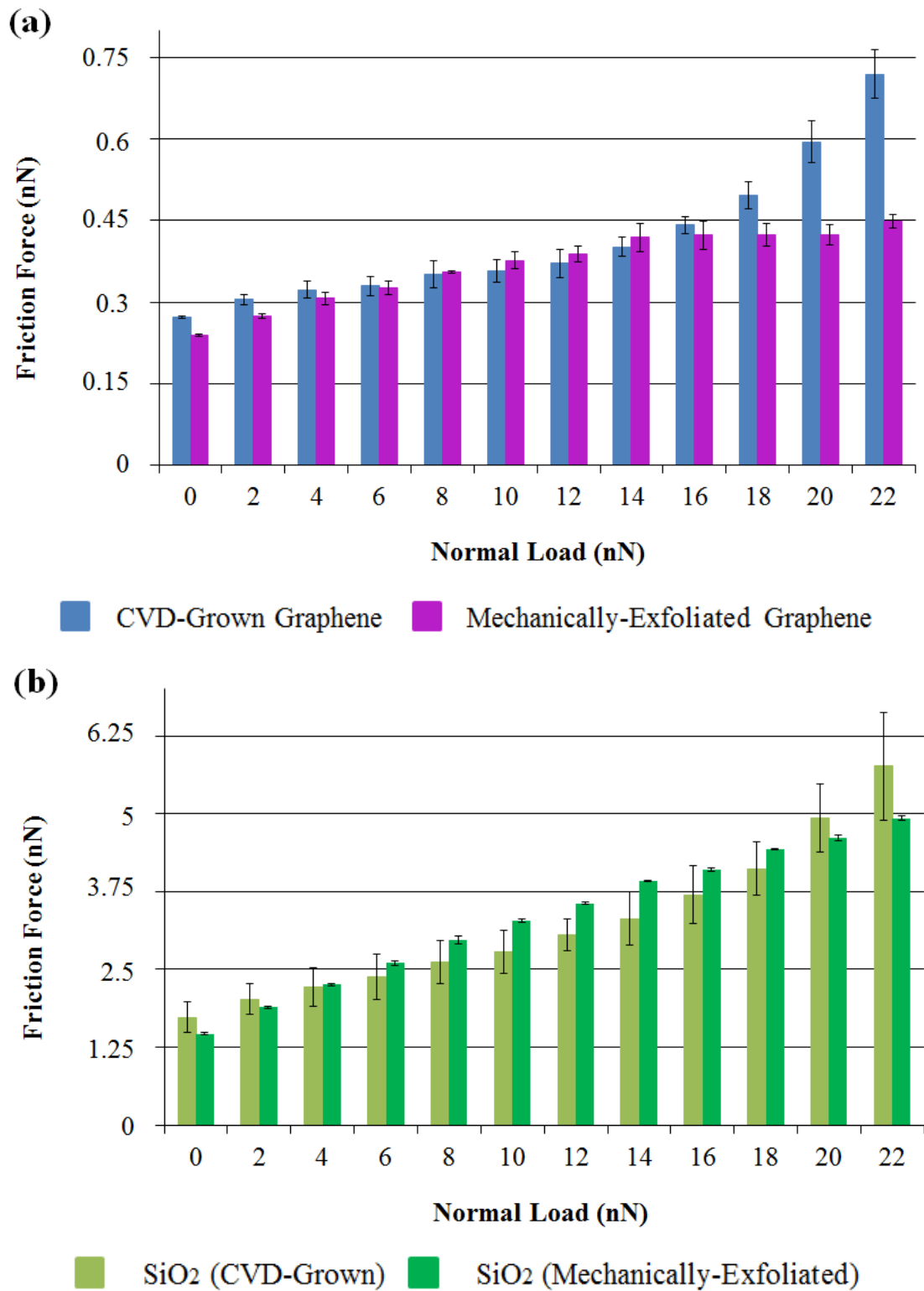
Figure 4.13 Graph detailing the dependence of friction force (F_f) on normal load (F_n) for (a) CVD-grown and mechanically-exfoliated graphene samples, and (b) the SiO$_2$/Si substrates on which they are situated. Data acquired with Tip 3.
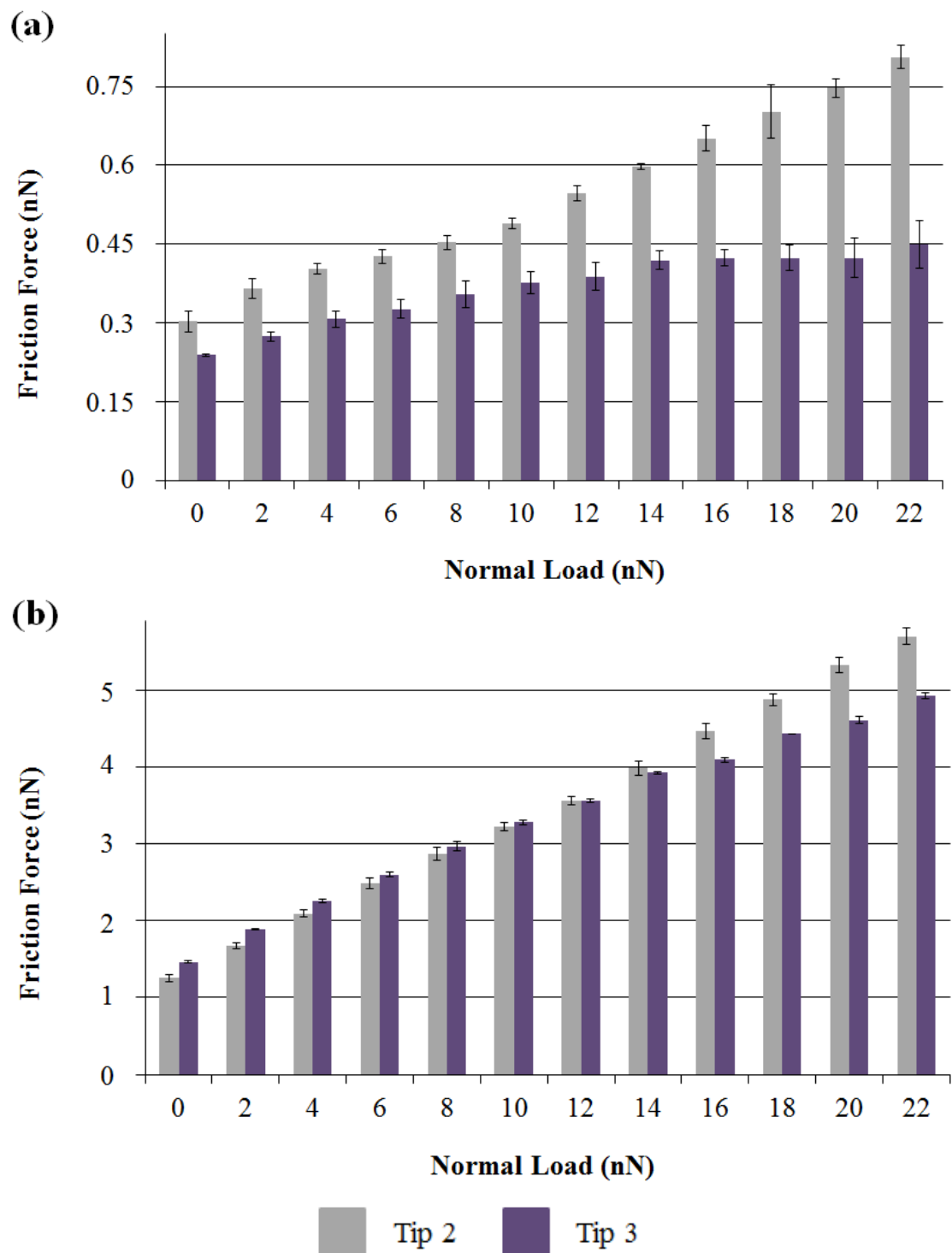
Figure 4.14 Graph detailing the dependence of friction force (F_f) on normal load (F_n) for (a) mechanically-exfoliated graphene, and (b) its SiO_2/Si substrate, for two different tips (Tip 2: grey, Tip 3: purple).

4.3.3 Lubrication Performance of CVD-Grown Graphene on SiO$_2$/Si Substrates

To prolong the life expectancy of any mechanical system that features moving components, wear and friction must be minimized via appropriate lubrication approaches. In the industry, graphite-based lubricants are widely utilized towards this purpose [77]. On the other hand, a major drawback of using graphite as a lubricant is that it requires a humid environment to function properly. It has been recently proposed that single-/few- graphene could replace graphite as the ideal solid lubricant, since their lubrication properties are not expected to depend heavily on humidity [77]. Additionally, graphene is largely impermeable towards many molecules, which would potentially lower the oxidation and corrosion of surfaces that it covers [78].

The ability to investigate in detail the tribological properties of CVD-grown graphene via the recording of lateral force maps at changing normal loads has been demonstrated in the previous sections of this chapter. In particular, it has been determined that the absolute friction values exhibited by graphene itself (as well as its wrinkles and the SiO$_2$/Si substrates on which the samples are situated) can be appreciably influenced by (i) the use of different AFM tips, and (ii) post-transfer cleaning procedures. As already indicated, rather than comparing absolute friction force values, it makes sense to employ *coefficient of friction* (μ) values (extracted from linear fits to F_f vs. F_n data) in evaluating graphene's tribological properties, to eliminate the influence of potential differences in adhesion behavior between graphene and SiO$_2$/Si substrates. Additionally, to eliminate the effect of using (i) AFM tips with different apex structures/chemistry, and (ii) potential changes in tip apex/structure during the experiments, it makes sense to determine *ratios* of coefficients of friction between graphene and the substrate ($\mu_{Graphene}/\mu_{SiO2}$), and obtain average values from results delivered by the different tips. In this way, ($\mu_{Graphene}/\mu_{SiO2}$) values represent a true *figure of merit* to evaluate the lubricative properties of graphene samples.

Based on the discussion above, ($\mu_{Graphene}/\mu_{SiO2}$) ratios for CVD-grown graphene in three variants (as-transferred, ultrasonic-cleaned, and Ar-gas-cleaned) as well as exfoliated graphene are provided in Table 4.2, for (up to) five different probe tips, together with mean and standard deviation values.

By examining the values reported in Table 4.2, it is seen that graphene in all examined forms acts as a very good solid lubricant, reducing the coefficient of friction observed on SiO_2/Si substrates by ~90%. Among CVD-grown graphene samples, the as-transferred variety exhibits the highest mean lubrication performance (thus, the lowest $\mu_{Graphene}/\mu_{SiO2}$ ratio) and the mean lubrication performance drops slightly with ultrasonic cleaning, while Ar-gas-cleaned samples exhibit the lowest mean lubrication performance. It should be mentioned that a consideration of standard deviation values together with the mean values reported for as-transferred and ultrasonic-cleaned samples indicates that there is no statistically-significant difference in overall lubrication performance between the two varieties of graphene. On the other hand, Ar-gas-cleaned samples clearly exhibit a comparatively lower lubrication performance. A potential physical mechanism responsible for this effect could involve the thermal breakdown of PMMA residue trapped *under* the transferred graphene samples during annealing, leading to a wide distribution of trapped contaminants increasing average surface roughness and friction. However, more experiments focusing specifically on high-resolution topography mapping should be performed in future work to clearly address this hypothesis.

Our results also allow a comparison of the lubrication performance of CVD-grown and exfoliated graphene samples. While it is seen that as-transferred CVD-grown graphene samples on average exhibit slightly better lubrication performance than exfoliated ones, the existence of wrinkles on CVD-grown graphene and the associated increase in friction should be taken account (please note that the data for CVD-grown graphene presented in Table 4.2 has been acquired on regions free from wrinkles). In that respect, the extent to which wrinkles increase friction values on CVD-grown graphene (as-transferred, ultrasonic-cleaned, and Ar-gas-cleaned) is examined in Table 4.3. As expected, wrinkles lead to a significant (about three-fold) enhancement of local friction values on CVD-grown graphene samples. It should be noted that the enhancement of friction on wrinkles is smallest for Ar-gas-cleaned samples, again presumably due to the "more even" distribution of PMMA residue under the graphene after annealing, reducing a potential concentration of contamination under the wrinkles.

Table 4.2 The ratios of coefficients of friction of graphene to SiO_2 ($\mu_{Graphene}/\mu_{SiO2}$)

	Tip 1	Tip 2	Tip 3	Tip 4	Tip 5	Mean	Standard Deviation
As-Transferred	0.07559	0.04183	0.10255	0.07849	-	0.07461	0.02497
Ultrasonic-Cleaned	0.06066	0.06786	0.08064	0.07992	0.10558	0.07893	0.01710
Ar-Gas-Cleaned	0.12364	-	0.11005	0.12348	-	0.11906	0.00780
Exfoliated	-	0.11041	0.05862	0.07226	0.14928	0.09764	0.04080

Table 2.3 The ratios of local friction forces measured on wrinkles to those on surrounding graphene ($F_{Wrinkle}/F_{Graphene}$). Data averaged over 10 wrinkles.

	Tip 1	Tip 2	Tip 3	Tip 4	Tip 5	Mean	Standard Deviation
As-Transferred	3.81365	3.48202	2.56946	3.37203	-	3.30929	0.52772
Ultrasonic-Cleaned	2.75695	2.79613	-	4.01650	4.01767	3.39681	0.71640
Ar-Gas-Cleaned	2.31252	-	2.89220	2.46706	-	2.55726	0.30018

Chapter 5

Summary and Outlook

This M.S. thesis presents the preparation of CVD-grown graphene on copper foils, as well as a comprehensive structural and nanotribological characterization of CVD-grown graphene transferred onto SiO_2/Si substrates. The results here make substantial contributions to the further understanding of frictional properties exhibited by the *two-dimensional* material graphene, and help to evaluate its potential as a solid lubricant in practical applications.

Specifically:

Among the various preparation methods of the graphene, the chemical vapor deposition (CVD) method has been selected due to its capability of providing high quality graphene of sufficiently large dimensions for practical applications. The process of sample preparation and post-preparation transfer onto SiO_2/Si substrates has been optimized via a series of experiments. Advanced microscopy techniques have been utilized for the structural and morphological characterization of the obtained graphene films. In particular, optical microscopy, scanning electron microscopy (SEM), and atomic force microscopy (AFM) have been used to inspect graphene coverage on the substrate and associated structural features. On the other hand, Raman spectroscopy has been extensively utilized to confirm the single-layer

character of CVD-grown samples and to judge sample quality in terms of the existence of microstructural defects.

Following the sample preparation and structural characterization phases of the experiments, the lubrication performance of CVD-grown graphene on SiO_2/Si substrates has been analyzed via atomic force microscopy (AFM) measurements in the friction force microscopy (FFM) mode, under ambient conditions and by using several calibrated cantilevers. In particular, the effect of various parameters such as using different probe tips, post-transfer cleaning procedures, and growth conditions on the nanotribological properties of CVD-grown graphene has been evaluated. Results indicate in general that CVD-grown graphene acts as a very good solid lubricant on SiO_2/Si, reducing coefficients of friction by ~90% for all investigated samples. It has been shown that as-transferred CVD-grown graphene exhibits the highest mean lubrication performance and that the associated values drop slightly with post-transfer cleaning. Finally, the effect of *wrinkles* associated with CVD-grown graphene on measured friction values have been quantitatively evaluated, with results revealing a substantial increase in friction on these structural defects.

While the experimental data presented here comprises substantial information on the nanotribological properties of CVD-grown graphene, further work is definitely needed to conclusively evaluate its suitability as a solid lubricant for practical applications, involving, e.g., micro- and nano-scale electro-mechanical systems. In particular, strategies aimed at reducing the number of wrinkles during sample preparation are expected to contribute substantially to the lubricative properties of this *two-dimensional* material.

Bibliography

[1] P. J. Blau, "Friction science and technology: from concepts to applications," *CRC Press*, Boca Raton, 2009.

[2] T. Mang, K. Bobzin and T. Bartels, "Industrial tribology: tribosystems, friction, wear and surface engineering, lubrication," *Wiley-VCH*, Weinheim, 2011.

[3] B. Bhushan, "Principles and applications of tribology," *John Wiley*, New York, 1999.

[4] G. Jianping, W. D. Luedtke, D. Gourdon, M. Ruths, J. N. Israelachvili and U. Landman, "Frictional forces and amontons' law: from the molecular to the macroscopic scale," *The Journal of Physical Chemistry B*, vol. 108, no. 11, pp. 3410-3425, 2004.

[5] J. Krim, "Surface science and the atomic-scale origins of friction: what once was old is new again," *Surface Science*, vol. 500, no.1-3, pp. 741-758, 2002.

[6] Image retrieved from: http://gizmodo.com/scientists-discovered-the-egyptian-secret-to-moving-hug-1569802879

[7] G. Binnig, H. Rohrer, C. Gerber and E. Weibel, "Surface studies by scanning tunneling microscopy," *Physical Review Letters*, vol. 49, no. 1, pp. 57-61, 1982.

[8] G. Binnig, C. F. Quate and C. Gerber, "Atomic force microscope," *Physical Review Letters*, vol. 56, no. 9, pp. 930-933, 1986.

[9] http://www.nobelprize.org/nobel_prizes/physics/laureates/1986/press.html

[10] J. N. Israelachvili and G. E. Adams, "Measurement of forces between two mica surfaces in aqueous electrolyte solutions in the range 0–100 nm," *Journal of the*

Chemical Society, Faraday Transactions 1: Physical Chemistry in Condensed Phases, vol. 74, pp. 975, 1978.

[11] C. M. Mate, G. M. Mcclelland, R. Erlandsson and S. Chiang, "Atomic-scale friction of a tungsten tip on a graphite surface," *Physical Review Letters*, vol. 59, no. 17, pp. 1942-1945, 1987.

[12] I. Szlufarska, M. Chandross and R. W. Carpick, "Recent advances in single-asperity nanotribology," *Journal of Physics D: Applied Physics*, vol. 41, no. 12, pp. 123001, 2008.

[13] H. P. Boehm, R. Setton and E. Stumpp, "Nomenclature and terminology of graphite intercalation compounds," *Carbon*, vol. 24, no. 2, pp. 241-245, 1986.

[14] K. S. Novoselov, A. K. Geim, S. V. Morozov, D. Jiang, Y. Zhang, S. V. Dubonos, I. V. Grigorieva and A. A. Firsov "Electric field effect in atomically thin carbon films," *Science*, vol. 306, no. 5696, pp. 666-669, 2004.

[15] K. S. Novoselov, D. Jiang, F. Schedin, T. J. Booth, V. V. Khotkevich, S. V. Morozov and A. K. Geim, "Two-dimensional atomic crystals," *Proceedings of the National Academy of Sciences*, vol. 102, no. 30, pp. 10451-10453, 2005.

[16] A. Geim, "Graphene: status and prospects," *Science*, vol. 324, no. 5934, pp. 1530-1534, 2009.

[17] K. S. Novoselov, A. K. Geim, S. V. Morozov, D. Jiang, M. I. Katsnelson, I. V. Grigorieva, S. V. Dubonos and A. A. Firsov, "Two-dimensional gas of massless Dirac fermions in graphene," *Nature*, vol. 438, no. 7065, pp. 197-200, 2005.

[18] C. Lee, X. Wei, J. W. Kysar and J. Hone, "Measurement of the elastic properties and intrinsic strength of monolayer graphene," *Science*, vol. 321, no. 5887, pp. 385-388, 2008.

[19] C. Lee, Q. Li, W. Kalb, X. Z. Liu, H. Berger, R. W. Carpick and J. Hone, "Frictional characteristics of atomically thin sheets," *Science*, vol. 328, no. 5974, pp. 76-80, 2010.

[20] T. Filleter, J. L. Mcchesney, A. Bostwick, E. Rotenberg, K. V. Emtsev, Th. Seyller, K. Horn and R. Bennewitz, "Friction and dissipation in epitaxial graphene films," *Physical Review Letters*, vol. 102, no. 8, pp. 086102, 2009.

[21] X. Li, W. Cai, J. An, S. Kim, J. Nah, D. Yang, R. Piner, A. Velamakanni, I. Jung, E. Tutuc, S. K. Banerjee, L. Colombo and R. S. Ruoff, "Large-area synthesis of

high-quality and uniform graphene films on copper foils," *Science*, vol. 324, no. 5932, pp. 1312-1314, 2009.

[22] C. Berger, Z. Song, T. Li, X. Li, A. Y. Ogbazghi, R. Feng, Z. Dai, A. N. Marchenkov, E. H. Conrad, P. N. First and W. A. D. Heer, "Ultrathin epitaxial graphite: 2D electron gas properties and a route toward graphene-based nanoelectronics," *The Journal of Physical Chemistry B*, vol. 108, no. 52, pp. 19912-19916, 2004.

[23] P. R. Somani, S. P. Somani and M. Umeno, "Planer nano-graphenes from camphor by CVD," *Chemical Physics Letters*, vol. 430, no. 1-3, pp. 56-59, 2006.

[24] A. Reina, X. Jia, J. Ho, D. Nezich, H. Son, V. Bulovic, M. S. Dresselhaus and J. Kong, "Large area, few-layer graphene films on arbitrary substrates by chemical vapor deposition," *Nano Letters*, vol. 9, no. 1, pp. 30-35, 2009.

[25] T. Oznuluer, E. Pince, E. O. Polat, O. Balci, O. Salihoglu and C. Kocabas, "Synthesis of graphene on gold," *Applied Physics Letters*, vol. 98, no. 18, pp. 183101, 2011.

[26] W. Li, Y. Ding, S. L. Suib, J. F. Dicario and F. S. Galasso, "Controlling the growth of CVD carbon from methane on transition metal substrates," *Surface and Coatings Technology*, vol. 190, no. 2-3, pp. 366-371, 2005.

[27] B. Hu, Z. Wei, H. Ago, Y. Jin, M. Xia, Z. Luo, Q. Pan and Y. Liu, "Effects of substrate and transfer on CVD-grown graphene over sapphire-induced Cu films," *Science China Chemistry*, vol. 57, no. 6, pp. 895-901, 2014.

[28] E. Koo and S. Ju, "Role of residual polymer on chemical vapor grown graphene by raman spectroscopy," *Carbon*, vol. 86, pp. 318-324, 2015.

[29] M. Kratzer, B. C. Bayer, P. R. Kidambi, A. Matković, R. Gajić, A. Cabrero-Vilatela, R. S. Weatherup, S. Hofmann and C. Teichert, "Effects of polymethylmethacrylate-transfer residues on the growth of organic semiconductor molecules on chemical vapor deposited graphene," *Applied Physics Letters*, vol. 106, no.10, pp. 103101, 2015.

[30] K. S. Kim, Y. Zhao, H. Jang, S. Y. Lee, J. M. Kim, J. Ahn, P. Kim, J. Choi and B. H. Hong, "Large-scale pattern growth of graphene films for stretchable transparent electrodes," *Nature*, vol. 457, no. 7230, pp. 706-710, 2009.

[31] S. Bae, H. Kim, Y. Lee, X. Xu, J.Park, Y. Zheng, J. Balakrishnan, T. Lei, H. R. Kim, Y. I. Song, Y.Kim, K. S. Kim, B. Ozyilmaz, J.Ahn, B. H. Hong and S. Iijima, "Roll-to-roll production of 30-inch graphene films for transparent electrodes," *Nature Nanotechnology*, vol. 5, no. 8, pp. 574-578, 2010.

[32] J. Song, F. Kam, R. Png, W. Seah, J. Zhuo, G. Lim, P. K. H. Ho and Lay-Lay Chua, "A general method for transferring graphene onto soft surfaces," *Nature Nanotechnology*, vol. 8, no. 5, pp. 356-362, 2013.

[33] Y. Lin, C. Jin, J. Lee, S. Jen, K. Suenaga and P.Chiu, "Clean Transfer of Graphene for Isolation and Suspension," *ACS Nano*, vol. 5, no. 3, pp. 2362-2368, 2011.

[34] V. K. Khanna, "Nanosensors: physical, chemical, and biological," *CRC Press*, Boca Raton, 2012.

[35] Y. Gogotsi and V. Presser, "Carbon nanomaterials," *CRC Press*, Boca Raton, 2014.

[36] C. Mattevi, H. Kim and M. Chhowalla, "A review of chemical vapour deposition of graphene on copper," *Journal of Materials Chemistry.*, vol. 21, no. 10, pp. 3324-3334, 2011.

[37] W. Whyte, "Cleanroom technology: fundamentals of design, testing, and operation," *John Wiley*, United Kingdom, 2010.

[38] G. H. Lee, R. C. Cooper, S. J. An, S. Lee, A. V. D. Zande, N. Petrone, A. G. Hammerberg, C. Lee, B. Crawford, W. Oliver, J. W. Kysar and J. Hone, "High-strength chemical-vapor-deposited graphene and grain boundaries," *Science*, vol. 340, no. 6136, pp. 1073-1076, 2013.

[39] M. Her, R. Beams and L. Novotny, "Graphene transfer with reduced residue," *Physics Letters A*, vol. 377, no. 21-22, pp. 1455-1458, 2013.

[40] A. Pirkle, J. Chan, A. Venugopal, D. Hinojos, C. W. Magnuson, S. Mcdonnell, L. Colombo, E. M. Vogel, R. S. Ruoff and R. M. Wallace, "The effect of chemical residues on the physical and electrical properties of chemical vapor deposited graphene transferred to SiO_2," *Applied Physics Letters*, vol. 99, no. 12, pp. 122108, 2011.

[41] Y. Dan, Y. Lu, N. J. Kybert, Z. Luo and A. T. C. Johnson, "Intrinsic response of graphene vapor sensors," *Nano Letters*, vol. 9, no. 4, pp. 1472-1475, 2009.

[42] C. Gong, H. C. Floresca, D. Hinojos, S. Mcdonnell, X. Qin, Y. Hao, S. Jandhyala, G. Mordi, J. Kim, L. Colombo, R. S. Ruoff, M. J. Kim, K. Cho, R. M. Wallace and Y. J. Chabal, "Rapid selective etching of PMMA residues from transferred graphene by carbon dioxide," *The Journal of Physical Chemistry C*, vol. 117, no. 44, pp. 23000-23008, 2013.

[43] C. W. Jang, J. H. Kim, J. M. Kim, D. H. Shin, S. Kim and S. Choi, "Rapid-thermal-annealing surface treatment for restoring the intrinsic properties of graphene field-effect transistors," *Nanotechnology*, vol. 24, no. 40, pp. 405301, 2013.

[44] V. Skákalová and A. B. Kaiser, "Graphene: properties, preparation, characterization and devices," *Woodhead Publishing*, Cambridge, 2014.

[45] A. C. Ferrari, J. C. Meyer, V. Scardaci, C. Casiraghi, M. Lazzeri, F. Mauri, S. Piscanec, D. Jiang, K. S. Novoselov, S. Roth and A. K. Geim, "Raman spectrum of graphene and graphene layers," *Physical Review Letters*, vol. 97, no. 18, 2006.

[46] T. F. Chung, T. Shen, H. Cao, L. A. Jauregui, W. Wu, Q. Yu, D. Newell and Y. P. Chen, "Synthetic graphene grown by chemical vapor deposition on copper foils," *International Journal of Modern Physics B*, vol. 27, no. 10, pp. 1341002, 2013.

[47] B. R. Shmaefsky, "Biotechnology 101," *Greenwood*, Westport, 2006.

[48] K. S. Saladin, "Human anatomy," *McGraw-Hill*, New York, 2008.

[49] C. S. S. R. Kumar, "Raman spectroscopy for nanomaterials characterization," *Springer*, Berlin, 2012.

[50] A. R. Rao, V. Hanchanale, P. Javle, O. Karim and H. Motiwala, "Spectroscopic view of life and work of the nobel laureate sir c.v. raman," *Journal of Endourology*, vol. 21, no. 1, pp. 8-11, 2007.

[51] J. R. Ferraro and K. Krishnan, "Practical fourier transform infrared spectroscopy: industrial and laboratory chemical analysis," *Academic Press*, San Diego, 1990.

[52] J. Goldstein, D. E. Newbury, D. C. Joy, C. E. Lyman, P. Echlin, E. Lifshin, L. Sawyer and J. R. Michael, "Scanning electron microscopy and x-ray microanalysis," *Springer*, Berlin, 2003.

[53] A. Bogner, P. H. Jouneau, G. Thollet, D. Basset and C. Gauthier, "A history of scanning electron microscopy developments: towards "wet-stem" imaging," *Micron*, vol. 38, no. 4, pp. 390-401, 2007.

[54] J. Lee, X. Zheng, R. C. Roberts and P. X.-L. Feng, "Scanning electron microscopy characterization of structural features in suspended and non-suspended graphene by customized CVD growth," *Diamond and Related Materials*, vol. 54, pp. 64-73, 2015.

[55] Z. Wang, G. Weinberg, Q. Zhang, T. Lunkenbein, A. Klein-Hoffmann, M. Kurnatowska, M. Plodinec, Q. Li, L. Chi, R. Schloegl and M. Willinger, "Direct observation of graphene growth and associated copper substrate dynamics by in situ scanning electron microscopy," *ACS Nano*, vol. 9, no. 2, pp. 1506-1519, 2015.

[56] I. N. Kholmanov, C. W. Magnuson, A. E. Aliev, H. Li, B. Zhang, J. W. Suk, L. L. Zhang, E. Peng, S. H. Mousavi, A. B. Khanikaev, R. Piner, G. Shvets and R. S. Ruoff, "Improved electrical conductivity of graphene films integrated with metal nanowires," *Nano Letters*, vol. 12, no. 11, pp. 5679-5683, 2012.

[57] R. Garcia and R. Perez, "Dynamic atomic force microscopy methods," *Surface Science Reports*, vol. 47, no. 6-8, pp. 197-301, 2002.

[58] P. Eaton and P. West, "Atomic Force Microscopy," *Oxford University Press*, New York, 2010.

[59] A. Das, B. Chakraborty and A. K. Sood, "Raman spectroscopy of graphene on different substrates and influence of defects," *Bulletin of Materials Science*, vol. 31, no. 3, pp. 579-584, 2008.

[60] A. Nourbakhsh, M. Cantoro, A. Klekachev, F. Clemente, B. Sorée, M. H. V. D. Veen, T. Vosch, A. Stesmans, B. Sels and S. D. Gendt, "Tuning the fermi level of SiO2-supported single-layer graphene by thermal annealing," *The Journal of Physical Chemistry C*, vol. 114, no. 15, pp. 6894-6900, 2010.

[61] Y. Lin, C. Lu, C. Yeh, C. Jin, K. Suenaga and P. Chiu, "Graphene annealing: how clean can it be?" *Nano Letters*, vol. 12, no. 1, pp. 414-419, 2012.

[62] K. Çelebi, "Chemical vapor deposition of graphene on copper", *Ph.D. Thesis*, ETH Zurich, 2013.

[63] H. Hölscher, A. Schirmeisen and U. D. Schwarz, "Principles of atomic friction: From sticking atoms to superlubric sliding," *Philosophical Transactions A*, vol. 366, no. 1869, pp. 1383-1404, 2008.

[64] Y. Peng, Z. Wang and C. Li, "Study of nanotribological properties of multilayer graphene by calibrated atomic force microscopy," *Nanotechnology*, vol. 25, no. 30, pp. 305701, 2014.

[65] T. Filleter and R. Bennewitz, "Structural and frictional properties of graphene films on SiC (0001) studied by atomic force microscopy," *Physical Review B*, vol. 81, no. 15, pp. 155412, 2010.

[66] P. Egberts, G. H. Han, X. Z. Liu, A. T. C. Johnson and R. W. Carpick, "Frictional behavior of atomically thin sheets: hexagonal-shaped graphene islands grown on copper by chemical vapor deposition," *ACS Nano*, vol. 8, no. 5, pp. 5010-5021, 2014.

[67] G. Fessler, B. Eren, U. Gysin, T. Glatzel and E. Meyer, "Friction force microscopy studies on SiO_2 supported pristine and hydrogenated graphene," *Applied Physics Letters*, vol. 104, no. 4, pp. 041910, 2014.

[68] K. S. Kim, H. Lee, C. Lee, S. Lee, H. Jang, J. Ahn, J. Kim and H.Lee, "Chemical vapor deposition-grown graphene: the thinnest solid lubricant," *ACS Nano*, vol. 5, no. 6, pp. 5107-5114, 2011.

[69] B. Bhushan, "Springer handbook of nanotechnology," *Springer-Verlag Berlin*, Heidelberg, 2004.

[70] M. Varenberg, I. Etsion and G. Halperin, "An improved wedge calibration method for lateral force in atomic force microscopy," *Review of Scientific Instruments*, vol. 74, no. 7, pp. 3362-3367, 2003.

[71] U. D. Schwarz, P. Koster and R. Wiesendanger, "Quantitative analysis of lateral force microscopy experiments," *Review of Scientific Instruments*, vol. 67, no. 7, pp. 2560-2567, 1996.

[72] J. E. Sader, I. Larson, P. Mulvaney and L. R. White, "Method for the calibration of atomic force microscope cantilevers," *Review of Scientific Instruments*, vol. 66, no. 7, pp. 3789-3798, 1995.

[73] U. D. Schwarz, W. Allers, G. Gensterblum and R. Wiesendanger, "Low-load friction behavior of epitaxial C 60 monolayers under hertzian contact," *Physical Review B*, vol. 52, no. 20, pp. 14976-14984, 1995.

[74] U. D. Schwarz, O. Zworner, P. Koster and R. Wiesendanger, "Quantitative analysis of the frictional properties of solid materials at low loads. I. carbon compounds," *Physical Review B*, vol. 56, no. 11, pp. 6987-6996, 1997.

[75] E. Meyer, R. Luthi, L. Howald, M. Bammerlin, M. Guggisberg and H. J. Guntherodt, "Site-specific friction force spectroscopy," *Journal of Vacuum Science & Technology B*, vol. 14, no. 2, pp. 1285-1288, 1996.

[76] S. Sundararajan, B. Bhushan, "Topography-induced contributions to friction forces measured using an atomic force/friction force microscope," *Journal of Applied Physics*, vol. 88, pp. 4825-4831, 2000.

[77] D. Berman, A. Erdemir and A. V. Sumant, "Graphene: a new emerging lubricant," *Materials Today*, vol. 17, no. 1, pp. 31-42, 2014.

[78] V. Berry, "Impermeability of graphene and its applications," *Carbon*, vol. 62, pp. 1-10, 2013.